Biomacromolecules

September/October 2003 Published by the American Chemical Society Volume 4, Number 5

Reviews

Quartz Crystal Microbalance: A Useful Tool for Studying Thin Polymer Films and Complex Biomolecular Systems at the Solution−Surface Interface

Kenneth A. Marx*

Center for Intelligent Biomaterials, Department of Chemistry, University of Massachusetts, Lowell, Massachusetts 01854

Received October 29, 2002

The quartz crystal microbalance (QCM) is a simple, cost effective, high-resolution mass sensing technique, based upon the piezoelectric effect. As a methodology, the QCM evolved a solution measurement capability in largely analytical chemistry and electrochemistry applications due to its sensitive solution-surface interface measurement capability. The technique possesses a wide detection range. At the low mass end, it can detect monolayer surface coverage by small molecules or polymer films. At the upper end, it is capable of detecting much larger masses bound to the surface. These can be complex arrays of biopolymers and biomacromolecules, even whole cells. In addition, the QCM can provide information about the energy dissipating properties of the bound surface mass. Another important and unique feature of the technique is the ability to measure mass and energy dissipation properties of films while simultaneously carrying out electrochemistry on solution species or upon film systems bound to the upper electrode on the oscillating quartz crystal surface. These measurements can describe the course of electropolymerization of a film or can reveal ion or solute transport within a film during changes in the film environment or state, including the oxidation state for an electroactive film driven by the underlying surface potential. The past decade has witnessed an explosive growth in the application of the QCM technique to the study of a wide range of molecular systems at the solution-surface interface, in particular, biopolymer and biochemical systems. In this report, we start with a brief historical and technical overview. Then we discuss the application of the QCM technique to measurements involving micellar systems, self-assembling monolayers and their phase transition behavior, molecularly imprinted polymers, chemical sensors, films formed using the layer-by-layer assembly technique, and biopolymer films and point out the utility of the electrochemical capabilities of the technique to characterizing film properties, especially electroactive polymer films. We also describe the wide range of surface chemistries and attachment strategies used by investigators to bring about surface attachment and multi-layer interactions of these thin film systems. Next we review the wide range of recent applications of the technique to: studies of complex biochemical and biomimetic systems, the creation of protein and nucleic acid biosensors, studies of attached living cells and whole cell biosensor applications. Finally, we discuss future technical directions and applications of the QCM technique to areas such as drug discovery.

Introduction

The development of new measurement techniques represents one of the major driving forces in biotechnology that positively impacts related research areas such as polymer characterization and biochemistry and is critical to the evolution of the pharmaceutical, biotechnology, and biomaterials industries. Indeed, the growing confluence of the previously unrelated disciplines of robotics, miniaturization

* To whom correspondence should be addressed. Phone: 978 934-3658. Fax: 978 934-3013. E-mail: kenneth_marx@uml.edu.

10.1021/bm020116i CCC: $25.00
Published on Web 08/13/2003

to the micro and nano scales, and signal transduction mechanisms applied to array technologies on surfaces combined with informatics has created a rapidly developing measurement technology area.[1] Some of the fastest growing applications have been in microarray technology at the micron scale applied to the study of cellular mRNA expression analysis (genomics) and cellular protein interaction/pathway analysis (proteomics).[2,3] These same techniques are also accelerating materials and catalyst design and identification.[4] At the heart of all such analysis techniques involving surfaces is some method for the immobilization of target or film to the surface and a signal transduction method for measuring the analyte bound or the material or process selected. The former requires the study and characterization of surface chemistries and often polymeric materials placed upon the surface to carry out immobilization. Furthermore, the latter requires a specific signal transduction mechanism, often involving an added label, either spectroscopic (e.g., absorption, fluorescence (most frequently), etc.), electroluminescent, chemileuminescent, or radiolabel. The quartz crystal microbalance (QCM) is an important technique that has unique advantages for addressing the problems and issues involved in developing these new measurement methodologies and applying them to complex biomolecular systems.

QCM Advantages. The advantages that the QCM provides for development of the above domain areas is a sensitive detection capability for surface mass binding and a surface viscoelastic characterization capability for the bound mass. Other distinct advantages of the QCM technique are the following. (1) The mass sensing technique eliminates the need for any specific labeling step to be part of the signal transduction mechanism. (2) Signal transduction via the piezoelectric mechanism operates well in complex, often optically opaque solution media. (3) The technique is capable of detecting subtle changes in the solution−surface interface that can be due to density−viscosity changes in the solution, viscoelastic changes in the bound interfacial material, and changes in the surface free energy, to name a few. (4) The electrochemical quartz crystal microbalance (EQCM) variant allows the investigator to apply a potential on the upper metal electrode, thereby creating an electrochemical cell, enabling electrochemical reactions or measurement of processes involving electron transfer. This provides interesting ways to create or probe surface bound mass as we describe in this review. (5) Finally, the technique is relatively easy to use, and the basic equipment is inexpensive to purchase.

Although the QCM will not supplant high throughput array technologies for drug or biomaterials screening, it provides the realistic possibility of low throughput arrays, perhaps useful in secondary screening situations. In this format, the QCM provides interesting ways to characterize the mass and viscoelastic properties of complex thin biopolymeric films incorporating biomolecular systems at surfaces in the solution of choice, both during their formation and once formed and under perturbations in their environment. Thus, the QCM technique becomes a useful adjunct to the development of future non-QCM array technologies. It has found use already as a gas phase chemical sensor and metal deposition sensor in vacuum applications and is being developed as a biosensor platform. For these reasons, the technique is currently exhibiting rapid growth outside of its traditional development domain area of analytical chemistry and electroanalytical chemistry. A number of review articles have appeared in recent years that discuss the applications and technical issues involved in QCM use. They range from the perspective of QCM as a fundamental tool in analytical electrochemistry[5] to comparative reviews focused on the newer application areas of biosensors[6−9] and drug discovery.[10] In this review, we concentrate on the application of the QCM technique to the study of the formation and characterization of thin but complex biopolymeric films and biomimetic systems involving biomacromolecules. We also briefly outline its applications to the study of fundamental biological processes, biosensors for analyte detection, and more complex biomolecular systems, including living cells.

Historical Overview. The signal transduction mechanism of the QCM technique relies upon the piezoelectric effect in quartz crystals, first discovered in 1880 by the Curie brothers, via a pressure effect on quartz.[11] A change in inertia of a vibrating crystal was then shown by Lord Rayleigh to alter its resonant frequency, f.[12] Important subsequent developments were good crystal stability through the use of electric resonators[13] and room-temperature stable AT-cut crystals.[14] In 1959, the QCM was first used in a sensing mode when Sauerbray reported a linear relationship between the f decrease of an oscillating quartz crystal and the bound elastic mass of deposited metal.[15] Early chemical applications of QCM were to measuring mass binding from gas-phase species to the quartz surface. These represented some of the earliest chemical sensors for moisture and volatile organic compounds,[16,17] environmental pollutants,[18] and gas-phase chromatography detectors.[19] In the 1980s, solution based QCM developed as new oscillator technology advanced to measure changes in frequency that could be related to changes in viscosity and density in highly damping liquid media.[20,21] The recent success of the QCM technique is due to its ability to sensitively measure mass changes associated with liquid−solid interfacial phenomena, as well as to characterize energy dissipative or viscoelastic behavior of the mass deposited upon the metal electrode surface of the quartz crystal.

Measuring Surface Film Mass, Viscoelasticity, Thickness, Hydrophilicity, and Roughness with QCM

QCM Device Features. By applying an alternating electric field across the quartz crystal through upper and lower metal electrodes covering the quartz surface, a mechanical oscillation of characteristic frequency, f, is produced in the crystal. Although the f range for the fundamental mode of quartz is between 5 and 20 MHz, most applications have used commercial QCM devices operating in the 5−10 MHz range. The 5−20 MHz frequencies produce device sensitivities to analytes that are comparable to a direct biosensing technique like surface plasmon resonance.[22] In addition, they provide information on the viscoelastic properties of bound mass. However, in routine usage, they cannot match the sensitivities of widespread optical techniques involving labeling with specific chromophores such as in fluoresence or chemile-

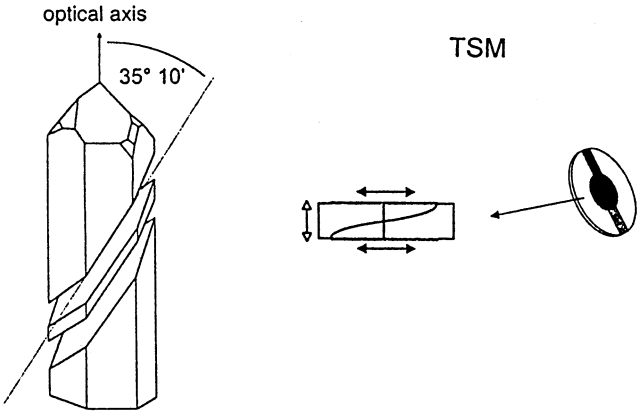

Figure 1. AT-cut of a quartz crystal from which the metal coated QCM quartz crystals are produced and an end on crystal view of the thickness shear mode (TSM) of oscillation. Reprinted with permission from ref 7. Copyright 2000 Wiley-VCH.

uminescence. These techniques are thoroughly compared in a comprehensive review.[7] Nonetheless, as we have already discussed, in some application scenarios, the QCM is overall comparable or superior to optical techniques.

Typically for QCM applications, quartz crystals a few tenths of a mm in thickness are cut in the AT form, at a 35° 10′ angle from the *Z*-axis as shown in Figure 1.[6,7,10] This geometry provides a stable oscillation with almost no temperature fluctuation in *f* at room temperature. In most applications, the QCM technique relies upon circular quartz crystals operating in the thickness shear mode (TSM) of oscillation, where motion lateral to the surface is as shown in Figure 1. Under these conditions, the lateral amplitude of a vibrating crystal is 1−2 nm. Any mass bound to the surface will tend to oscillate with the same lateral displacement and frequency as the underlying crystal. If it does so elastically, then there is no energy loss for this process. If energy loss accompanies this mass oscillation, then the process is said to be inelastic. The solution penetration depth of the lateral shear wave resulting from the oscillating crystal is 0.25 μM perpedicular to the upper surface at 20 °C.[7] This rapid attenuation of the shear wave energy is caused by the viscous damping forces of the solution.

The electrodes shown in Figure 1 can be one of a number of metals (Au and Pt, to name a few in widespread use) deposited upon the upper and lower quartz surfaces. Wire leads, attached to the electrodes (not shown), are then connected to an oscillator circuit. Typically, the continuous resonance mode is utilized, where relative shifts in crystal *f* are measured. A number of QCM devices are commercially available from the following vendors: Elchema, EG&G, QCM Research, Maxtek, and Universal Sensors.[5,6,23] We present in Figure 2 a schematic outline of a commercially available device from EG&G in which the crystal is contained in place via O-rings within a Teflon well holder, where the upper and lower portions of the well holder are secured together with screws.[24] In this specific application, the QCM device has been placed inside a cell culture incubator so that living cells may be studied attaching to the QCM gold surface. In this example, measurements were made of *f* and admittance, *A*, yielding the motional resistance, *R*, at the crystal−solution interface.

In general, samples in liquid aliquots can be delivered directly to the QCM electrode surface via syringe or micropipet to the liquid cell. Or in automated systems, flow injection analysis systems can deliver small volumes under laminar flow conditions to minimize mechanical influences on the QCM performance. Flow through cells have been described as well as systems where the QCM is mounted vertically on the side wall of a liquid cell.[25]

Elastic Mass Measurement. An increase in mass bound to the quartz surface causes the crystal's oscillation frequency to decrease. For the situation of pure elastic mass added to the surface, the well-known linear Sauerbray equation was first observed[15] and used to precisely quantify, with ng sensitivity, the quantity of elastic mass added to the surface

$$\Delta f = -2\Delta m f^2/A(\mu\rho_q)^{0.5} = -C_f\Delta m \qquad (1)$$

where Δf is the measured resonant frequency decrease (Hz), *f* is the intrinsic crystal frequency, Δm is the elastic mass change (g), *A* is the electrode area (0.196 cm^2 in many applications), ρ_q is the density of quartz (2.65 g/cm^3), and μ is the shear modulus (2.95×10^{11} dyn/cm^2). This results in C_f, the integrated QCM sensitivity, having a value of 0.903 Hz/ng for a ∼9 MHz crystal. Given this integrated sensitivity level, nearly 1000 times greater than an electronic mass balance with a sensitivity of 0.1 ug, this mass sensing technique has sometimes been termed the quartz crystal nanobalance. The Sauerbray equation is valid only for small elastic masses added to the crystal surface. It becomes inaccurate for masses greater than about 2% of the crystal mass.

Because mass is the most obvious factor affecting the *f* of an oscillating crystal, many investigators design their systems in order to maximize the bound mass change to be detected. Often, the strategy will be to design a mass amplification feature into the signal to be transduced by the crystal. For example, if one is studying an enzyme biosensor immobilized on the QCM surface, an optimal sensitivity approach may be to use a substrate that when catalytically converted to product by a high turnover number enzyme forms an insoluble precipitated mass on the QCM surface, decreasing *f* significantly.[26] In another example extending this approach, the electron-transfer resistance due to the mass of an insulating precipitate that resulted from an enzyme biosensor was measured and correlated with the mass precipitated as part of the biosensor signal calibration.[27]

In liquid-phase measurements, the QCM is not a simple mass sensor, but provides valuable information about reactions and conditions at the liquid−solid interface. In many of the applications of the QCM described below, where investigators have studied: deposited polymeric films, electrochemically created polymeric films, biomacromolecular film composites comprised of proteins and nucleic acids, and biosensors, including those comprised of living cells, the systems studied do not behave as elastic masses on the QCM surface. In these cases, the Sauerbray equation does not apply, and it is difficult if not impossible to extract corresponding mass binding quantities from decreases observed in the crystal *f* magnitude. This energy dissipating

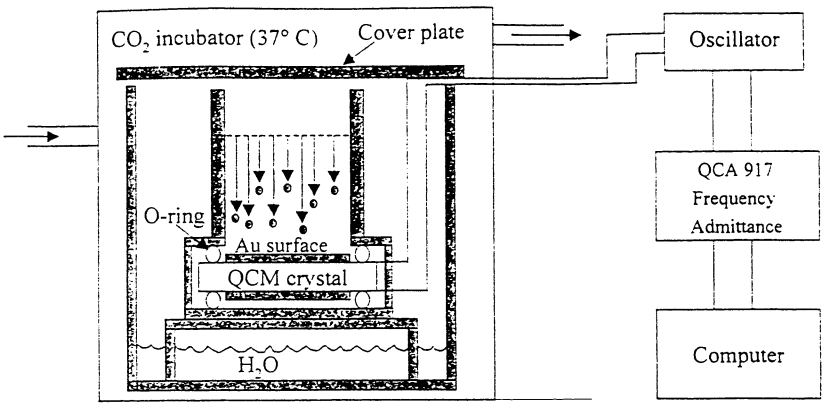

Figure 2. Schematic of a QCM crystal in its well holder and associated electronic components for automated *f* and *R* acquisition. In this example, the device resides in a cell culture incubator and cells are shown placed in media and serum above the crystal surface in a cell attachment study. Reprinted with permission from ref 24. Copyright 2000 American Chemical Society.

property of many inelastic systems under study is important to be able to document and characterize. We now discuss a number of QCM methods that have been developed that lead to information about the viscoelastic properties of the deposited film mass and to understanding how the substrate surface properties affect the measured parameters.

Pure Elastic Mass, Energy Dissipating Systems, and the Liquid Viscosity−Density Response. When one face of a quartz crystal is in contact with a liquid, its *f* and *R* values are affected by the liquid density and viscosity. Therefore, independent changes in the *f* response of a QCM crystal can be brought about singly or by a combination of (1) a pure elastic mass bound tightly to the QCM surface, where R is constant and the Sauerbray eq 1 holds; (2) a pure liquid viscosity−density change in the solution adjacent to the QCM surface, bringing about a change in both *f* and *R* in the presence or absence of mass binding; (3) the surface bound mass is inelastic and dissipates energy. In the latter case, there will be an *f* decrease due to both mass binding and to its viscoelastic energy dissipation behavior and *R* will increase.

In the first case, the Sauerbray eq 1 can be used to calculate elastic mass upon the QCM surface only after it has been determined experimentally that the bound mass dissipates no energy. Then, the *f* decrease of the dried mass can be used to calculate the bound mass. Assuming or knowing the dried film density allows the film thickness to be calculated. Alternately, if an electrochemical measurement of deposited mass is being made, the total charge passed at the electrode surface can be combined with the molar mass of the species involved, along with the electron redox stoichiometry at the electrode, to calculate the deposited mass and from this the film thickness. Or, as happens in some studies, film thickness may be determined or the QCM determined film thickness value validated using a totally different technique, for example, ellipsometry.

To determine what type of change is bringing about any given *f* change, the Δf, ΔR QCM data can be combined in the type of plot shown in Figure 3. A pure elastic mass binding, resulting in a decrease in *f*, has $\Delta R = 0$, and would exhibit the behavior shown by the horizontal line labeled from B to C. A pure liquid viscosity−density response has the *f* and *R* behavior shown by the dotted line labeled from A to D. This results from viscous coupling of the solution to the crystal, so that the solution effectively adds a mass component to the oscillating crystal. Assuming no slip between the solution and the crystal surface, that situation results in the following relationship. The equation for the resulting resonant frequency change was first derived by Kanazawa et al.[28] as follows:

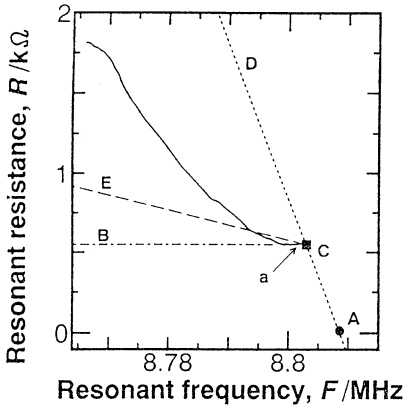

Figure 3. *f* (*F*) and *R* diagram for the electrochemical deposition of polypyrrole at constant current density. The point labeled C is the time zero starting point for polypyrrole electropolymerization, which is shown by the solid line moving to the left as synthesis proceeds. As a reference, pure elastic mass binding, resulting in a decrease in *f*, has $\Delta R = 0$, and would exhibit the behavior shown by the horizontal line labeled from B to C. A pure liquid viscosity−density response has the *f* and *R* behavior shown by the dotted line labeled from A to D. Reprinted with permission from ref 30. Copyright 1995 Elsevier.

$$\Delta f = -f^{3/2}(\rho_L \eta/\pi\mu\rho_q)^{1/2} \quad (2)$$

where ρ_L is the density of the liquid and η is the viscosity of the liquid. When the QCM operates in solution, the total *f* decrease cannot be deconvoluted into a contribution from a bound mass distinguishable from the solution contribution. For the quartz crystal in contact with liquid, the resonant resistance change was first derived by Muramatsu et al.[29] as follows:

$$\Delta R = (2\pi f \rho_L \eta)^{1/2} A/k^2 \quad (3)$$

where *k* is the electromechanical coupling factor. Because both Δf and ΔR are proportional to $(\rho_L\eta)^{1/2}$, the $\Delta f - \Delta R$ plot

is a straight line for liquids of different density and viscosity. For a series of different weight percent (0−46%) sucrose solutions, of varying density and viscosity, the *f* decrease and *R* increase can be determined relative to those of pure water using eqs 2 and 3 and can be fitted with a linear relationship.

Clearly, the behavior of specific systems under investigation can be graphically compared on such a plot and the relative viscoelastic behavior or energy dissipating properties of surface bound polymeric films or biomacromolecules can be assessed relative to liquid solution density−viscosity changes. The experimental example presented in Figure 3 illustrates this point. Here, an electrochemical deposition of a polypyrrole film is being carried out, and the output from measurements by a 9 MHz crystal are displayed. Electropolymerization starts at point C and is represented by the solid line moving to the left with time as synthesis proceeds.[30] The short horizontal region labeled a, lying along the line labeled B to C of zero slope (Sauerbray eq 1 behavior), shows *f* decreasing, whereas *R* is constant. This is where the electropolymerizing film behaves elastically. However, the subsequent electropolymerization rapidly changes behavior to a negative slope where the *f* decrease due to increasing film mass is accompanied by an *R* increase. This is the region where the film begins dissipating energy, exhibiting viscoelastic behavior. Using this approach, these investigators have provided criteria for evaluating the viscoelastic properties of films.[30] In contrast to this view of understanding film properties in relation to liquid phase properties, a purely experimental method using an appropriate FIA system has been proposed to suppress the side effects of fluid properties upon the QCM signal resulting from analyte adsorption.[31,32]

Surface Hydrophilicity and Roughness. There exists an interplay between the roughness and relative hydrophilicity of a QCM surface that affect the measured *f* and *R* values in a given experiment. During adsorption of mass to the QCM surface, an alteration in the hydrophilicity of the surface can result in large changes in *f*. Surfaces that are hydrophilic and rough can entrap liquids within surface cavities contributing to the mass increase sensed by the QCM. On the other hand, hydrophobic cavities often do not wet and air or vacuum can be entrapped. This results in smaller measured mass and energy losses. Therefore, when operating in liquids, the QCM surface must be smooth to avoid spurious effects from surface roughness and varying surface energies. To the extent that these quantities are not controlled or taken into account in the experimental design, the results obtained may not be able to reliably yield even semiquantitative information about the system being investigated.

A number of reports have documented the effect of relative surface hydrophobicity on the attached mass. As an interesting example, it is well-known that attachment dependent living cells are particularly sensitive to the properties of the underlying surface and will only thrive if the surface is sufficiently hydrophilic. Different cell density behavior of *f* decreases and *R* increases has been reported for normal endothelial cells during their attachment process to a steady state on the QCM surface when the gold surface is hydrophilic vs hydrophobic under media and serum.[33]

One approach to characterizing the relative surface hydrophobicity has been pioneered by a discontinuous resonance method.[34] These investigators' approach is to intermittently disconnect the oscillation, resulting in an exponentially decaying signal. The dissipation factor, *D*, inversely proportional to the decay time, is measured. This has been shown to be different for hydrophilic vs hydrophobic surfaces in the case of living cells on the QCM surface.[35] With this technique, information concerning the surface roughness can also be obtained as well as the energy dissipating viscoelastic properties of materials on the QCM surface.

One additional feature of QCM operation worth mentioning is the occurrence of longitudinal acoustic waves. These are standing compression waves traversing the distance of the solution between the QCM surface and the solution meniscus and being reflected back to the QCM surface. If there is appreciable evaporation from the solution, then this distance decreases with time and a time dependent alternating *f* and *R* oscillation will be measured. This oscillation is due to the changing path length for the standing wave. The time between peaks of this oscillation is the time required for evaporation of a lamella of solution that corresponds to one-half of a wavelength of the standing wave. The fundamental physics and experimental characterization of this phenomenon has been reviewed elsewhere.[7] Experimentally, this effect can be eliminated in a flow injection system or if the QCM is covered to eliminate evaporation during operation.[24]

Equivalent Circuit Analysis. As we stated above, when the QCM operates in solution, the total *f* decrease cannot be deconvoluted into a contribution from a bound mass distinguishable from the solution contribution. To do this requires a more complex series of measurements and characterization of the system with an electrical equivalent circuit model. Circuit analysis involves the operation of an impedance analyzer in tandem with the QCM transducer. Both impedance and admittance data can be collected and analyzed via fitting to an equivalent electrical circuit model.[36] What results are capacitance, resistance, and inductance data in addition to series and parallel frequencies to represent the properties of individual molecular components assembled on the crystal surface.[7,29,37,38] The impedance analysis of film systems on the QCM surface can result in greater insights into the viscoelastic properties of important complex materials, such as polyacrylamide films,[39] blood clots,[40] etc. However, these analyses are time-consuming and the equipment is relatively expensive. Moreover, the equivalent circuit models are approximate representations of the behavior of the bound mass under liquid. Therefore, these approaches have not found wide use, and we do not discuss them further in detail in this review. Instead, we refer the reader to the excellent discussions of this topic in two reviews that we have already cited.[7,9] However, in this review, we do present some results from specific studies in which these techniques have been applied.

QCM Studies of Biopolymer Film Formation, Viscoelastic Behavior, and Ion/Solute Transport Properties

The QCM device represents a simple and valuable tool with which to investigate the formation or degradation of biopolymeric films or film composites at a surface−solution interface in which single or multiple assembly steps are required. Either the kinetics (k_{assoc} or k_{dissoc}) of the process steps may be followed or more simply the equilibrium states. An important advantage of the QCM technique is that these studies can be performed where optical techniques are precluded. There are many experimental situations, for example in complex systems involving surfactants, self-assembling molecules, or biopolymers, where optically clear solutions cannot be achieved. Moreover, an additional advantage of the QCM is that not just the film mass but the viscoelastic or energy dissipation behavior of the film can simultaneously be measured during formation or at equilibrium. One final type of measurement for which the QCM provides unique information is the investigation of ion transport in charged films, including polymers, during changes in the film environment or oxidation state. The latter is carried out at a given electrochemical potential applied at the underlying EQCM electrode.

Because there is a broad continuum of systems under study that involve polymeric substrates and biological macromolecules (biosensors in many cases), we discuss systems and studies dominated by the biological component or biological analyte detection in a following major section on biosensors. It is our intent in this section to describe the uses of QCM to study systems focused on the polymeric film component. Investigators have applied the QCM technique to a variety of systems, some of which we describe below. These include electrochemical polymerization, conducting polymers, electroactive film redox properties, ion and solvent transport in films, micelle formation, enzymatic polymerization of micelles, LB monolayers, self-assembling monolayers, molecularly imprinted polymer films, nanoarchitecture, and layer-by-layer films.

Electropolymerization, Electroactive Film Studies, and Ion/Solvent Transport. Much of the development of the QCM technique in the field of analytical electrochemistry was driven by its high sensitivity for mass sensing at an electrode surface during electrochemical processes at an applied potential, EQCM. That attractive feature of the EQCM continues to be utilized in the study of polymeric films, including electropolymerization studies. Examples of the wide range of electropolymerization systems studied include phenols,[41] reversible C_{60} films,[42] a 32 unit ferrocenyl dendrimer,[43] methacrylonitrile film adsorption and desorption,[44] tyrosine derviative biofilm formation via electropolymerization vs adsorption,[45−47] and formation of conducting polymer films such as polypyrrole for fundamental investigations,[48−50] as well as pyrrole-biotinylated pyrrole co-electropolymerization for subsequent hierarchical structure creation, as in DNA attachment.[50,51] In Figure 3, we have already presented an example of the electropolymerization of polypyrrole and how the film can be determined to change from elastic behavior early in the polymerization process to exhibiting visoelastic, energy dissipating properties during the subsequent synthesis of a thicker film.

The details of ion and solvent transport between the film and solution can be sensitively followed using the EQCM. Typically, this is as a result of changes due to an applied potential. We discuss a number of representative examples. Within electropolymerized polypyrrole films, the macromolecular polyanion DNA (a 20−30 mer) has been incorporated as a counterion.[52] These films have DNA as the sole anion dopant during film formation. However, their electrochemically driven ion exchange properties are dominated by the small solution electrolyte cation because DNA cannot readily be expelled from the polypyrrole network. In another study, the oxidation of an $Os(bipy)_3^{2+}$ complex reversibly immobilized in a permselective Nafion film produced reversible f (mass) changes because of solvated cations in the supporting electrolyte.[53] Polyvinylferrocene films undergoing reversible oxidation−reduction exhibited reversible f (mass) changes.[54] Because the f change, Δf, for an elastic film can be related to concentration changes in any small diffusing species that changes in the film, the following eq 4 applies. Here Δf is related to the apparent molecular weight (MW) of the diffusing species giving rise to a total charge, Q, passed during the electrochemical change at the applied potential:

$$\Delta f = \mathrm{MW} C_f Q / nF \qquad (4)$$

Therefore, using eq 4, the MW of the species changing in the polyvinylferrocene film was experimentally determined and confirmed to be electrolyte anions PF_6^-, incorporated into the film during oxidation. In another example of this approach, a monolayer film of ferrocenylundecanethiolate was reversibly oxidized and the reversible increase in mass measured via the f change was calculated to be 430 g/mol.[55] Although the anion ClO_4^- only had a molar mass of 99.5 g/mol, these investigators interpreted the excess mass change as due to the simultaneous incorporation of water into the film along with the anion. It must be cautioned that the interpretations of f changes for a film in terms of ion or solvent flux can only be made if it has been established experimentally that no change has occurred in the energy dissipation properties of the film during the process under consideration. A change in film viscoelastic behavior could give rise directly to f shifts.

In another study, very different ion transport effects, measured as f shifts during cyclic sweeping of the potential, were noted for two related electropolymerizing biofilms.[47] These data are presented in Figure 4 for three successive cyclic potential sweeps. One film was polytyrosine, electropolymerized from the monomer, the amino acid tyrosine. The other was polydecyltyrosine, electropolymerized from the monomer, the decyl ester derivative of tyrosine (DEDT). The former, a charged species, exhibited modest film growth, measured in the EQCM as a decreasing f, on a Pt electrode with each potential cycle. The regular f decrease occurred during a specific portion of the potential cycle and little variation in f was observed during the other potential ranges of each cycle. In contrast, the DEDT film, showed little net mass change during successive potential cycles, but a large rapid overall f decrease, independent of cycling, that indicated

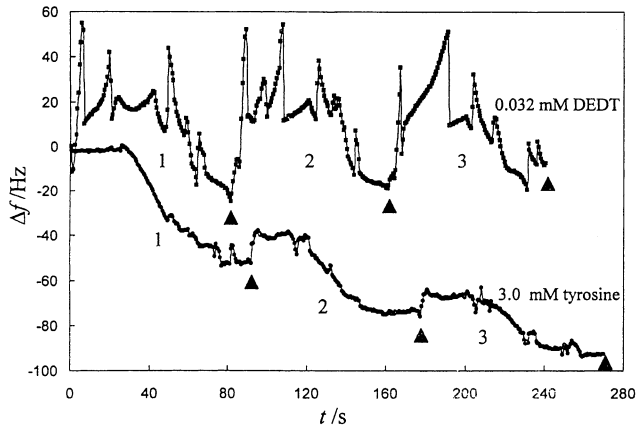

Figure 4. Potential dependent EQCM Δf shifts measured on Pt during cyclic voltammetry following a preadsorption phase with DEDT (decyl ester of D-tyrosine) and tyrosine monomers. The arrowheads indicate the approximate beginning and end times of 3 adjacent c.v. cycles (between 200 and 1000 mV; Ag/AgCl ref.) in the two monomer polymerization experiments. Reprinted with permission from ref 47. Copyright 2002 Elsevier.

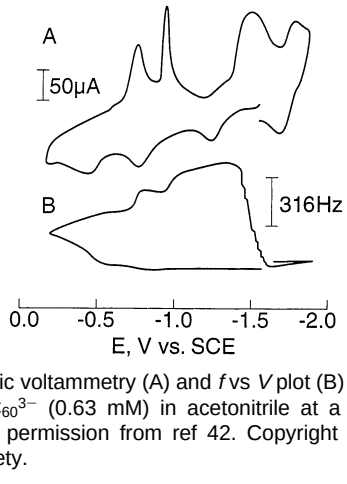

Figure 5. Cyclic voltammetry (A) and *f* vs *V* plot (B) for a solution of electroactive C_{60}^{3-} (0.63 mM) in acetonitrile at a gold electrode. Reprinted with permission from ref 42. Copyright 1992 American Chemical Society.

a significant level of adsorption to Pt via the known decyl chain dependent self-assembly properties of these monomer and polymeric species.[56,57] Moreover, during the potential cycling to form DEDT in Figure 4, 4−6 sharp fluctuations in *f* can be observed consistently at distinct potentials in successive cycles. These properties indicate that a complex flow of ions/water exists at certain potentials in the polydecyltyrosine film but are absent in the polytyrosine film.

Details of the reversible film formation and ion transport were observed in the case of an EQCM study of electroactive C_{60} films formed from C_{60}^{3-}. In this system, shown in Figure 5, three diffusion-controlled oxidations were observed during cyclic voltammogram sweeps of the type shown in panel A.[42] No film deposition was measured during the first and second oxidation peaks, but a significant amount was observed during the third that corresponded to the formation of the neutral species. Correlating the charge passed at the electrode with the *f* change at a constant potential, these investigators concluded that the film consisted of only the neutral C_{60} species, absent solvent or electrolyte ions. On reversing the potential scan, the mass increases observed were thought to be due to incorporation of electrolyte counterions into the increasingly anionic C_{60} films needed to maintain electrical neutrality. Return of the *f* to its initial value with the third reduction indicated that the film was completely dissolved, the C_{60}^{3-} species being completely solubilized.

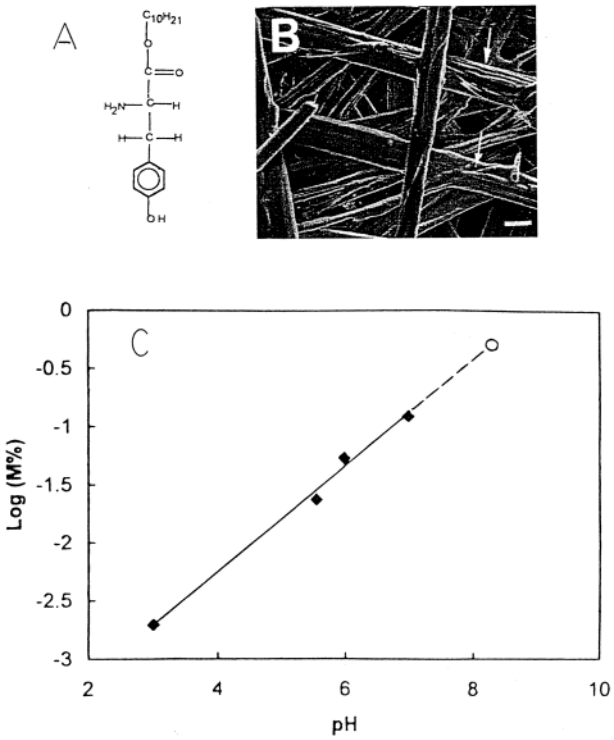

Figure 6. DEDT monomer structure shown in A and light microscopic image of the self-assembled structures formed by the monomer shown in B. The panel C figure plots DEDT binding data from QCM experiments using eq 1 to calculate approximate bound mass % as a function of varying the solution pH. The linear fitted solid line is shown extrapolated (dashed line) to the empty circle point where $(DEDT_m^+) = (DEDT_{aggr})$. This corresponds to the approximate pK_{app} for this equilibrium. Reprinted with permission from ref 45. Copyright 1999 American Chemical Society.

Micellar−Polymer Film Systems. The QCM technique has been applied to study a number of self-assembling systems, including surfactants that self-assemble from solution to form extended rodlike multilayer structures,[45−47,56,57] micellar interactions with polymeric films,[58−60] a helical polypeptide brush assembly on gold,[61] and micellization influences on the adsorption and electrochemistry of alkyl ferrocene surfactants.[62,63] Next we discuss some of the more interesting examples of this class of studies.

The decyl ester of the amino acid tyrosine is an amphiphilic species that self-assembles in solution above its cmc to form extended rodlike structures.[56,57] This system, containing the titrable amine group shown in Figure 6A, was studied in the QCM above its cmc. The self-assembly and gold surface binding kinetic behavior were followed as a function of the solution pH. A dramatic decrease in *f*, due largely to surface mass increase, was observed as the pH was raised from 5.0 to 7.0.[45] This corresponded to the deprotonation of the amine and self-assembly of the rodlike structures, shown in Figure 6B, due to decyl chain association. In Figure 6C are presented the *f* decrease levels for this system at different pH values, converted to corresponding bound mass levels. The authors were justified in doing so by the observed lack of change in *R* (data not shown), indicating elastic mass behavior, for the system at the three

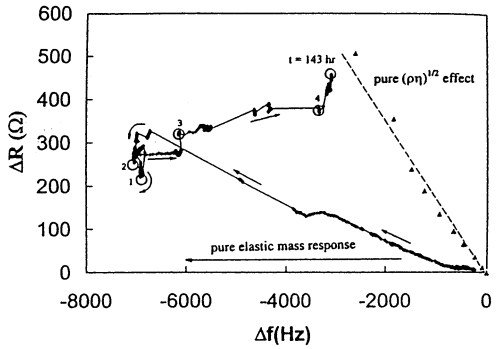

Figure 7. $\Delta f-\Delta R$ diagram of the time course of DEDT monomer aggregates binding to the QCM surface is shown, starting at $\Delta f = 0$ and following arrows. At point 1, horseradish peroxidase was added, and at points 2 through 4, successive hydrogen peroxide aliquots were added to carry out polymerization. After a total of 143 h of polymerization, the final point was reached. The pure elastic mass (solid line) and pure density−viscosity $(\rho\eta)^{0.5}$ (dashed line) effect lines are shown. The triangles represent the experimental values determined for solutions of increasing sucrose concentrations. Reprinted with permission from ref 45. Copyright 1999 American Chemical Society.

lowest pH values shown. Only at the highest pH value did the observed system *R* values increase during the time course of the experiment. Therefore, from Figure 6C, we observed an apparent p*K* of 8.3, estimated by extrapolation for the combined deprotonation and self-assembly equilibrium constant, in agreement with data from underivatized amino acid studies and from direct titration studies of the monomers. In Figure 7, for the highest system pH studied, starting at $\Delta f = 0$, it is clear that the kinetics of the self-assembly equilibrium demonstrated an initial 1 h phase in which the bound mass behaved elastically on the QCM gold surface. Then, over the next 24 h, as mass continued to add to the gold surface, the film exhibited energy dissipation behavior, as we alluded to above. Interestingly, the film, comprised of aggregates of self-assembled monomers, was shown to be enzymatically polymerizable using horseradish peroxidase. The enzymatic reaction could be followed solely with the QCM, because the equilibrium film behavior increased its viscoelastic properties during the reaction, as hydrogen peroxide was added stoichiometrically to carry out the reaction until polymerization was finished (transition from point 1 to 4 in Figure 7). This property demonstrates an advantage of the QCM, the ability to follow an enzymatic reaction under conditions of an optically opaque solution. An example of the QCM being used to follow the opposite process, enzymatic degradation of a polymer, has also been reported.[64]

An example of the interaction of a microemulsion with an immobilized biopolymer studied with the QCM is illustrated by the following report. The electrochemical and catalytic properties of a covalently immobilized vitamin B12 hexacarboxylate−polylysine film were found to be influenced by the sodium dodecyl sulfate microemulsion composition.[59] Fast catalytic turnover for dibromocyclohexane to cyclohexene was found to be facilitated by high conductivity, because of salt content and low viscosity of the microemulsion. In another study, small unilamellar vesicles were adsorbed to gold to form a monolayer film of vesicles that was then used as a substrate to bind a PEO−PPO−PEO triblock copolymer. The equilibrium binding of triblock copolymer was found to follow a Freundlich type of isotherm, and the kinetic properties of the system were found to correlate with increased membrane permeability of the vesicles induced by binding of the triblock copolymer.[60]

A system comprised of varying alkyl chain length quaternary amine ferrocene redox surfactants binding to gold was studied with the EQCM.[62] The reduced ferrocene derivatives were found to be more strongly adsorbed to the gold on the quartz surface than the oxidized species. From the adsorption isotherms, the ΔG of both redox forms were calculated. Differences in the formal potentials of the monomers free in solution and in micelles were shown to be functions of ΔG and the aggregation number for micellization. This allowed calculations of ΔG values for micellization of the surfactants.

Self-Assembled Monolayer Adsorption, Langmuir−Blodgett Monolayer Films, and Phase Transition Behavior. Some monolayer films formed via adsorption are considered to be examples of molecular self-assembly, such as the high affinity, organized alkane thiol monolayer films. A number of self-assembled monolayer and Langmuir−Blodgett (LB) monolayer films have been investigated with the QCM. For example, thiol and surfactant self-assembly kinetics and dynamics to form organized monolayers on gold surfaces have been studied.[38,65−68] In many instances, these systems are created and studied as the first of a number of steps in the design of higher order structures containing biological recognition elements. In the case of LB films, these have been studied with the QCM to discover how fundamental properties of the monolayer film change during the phase transition.[30,69] Next, we present some interesting examples of where these monolayer films have been investigated with the QCM.

Self-assembling monolayers based upon thiol reactivity with the gold surface of typical QCM crystals represents a relatively new class of devices to which biological recognition elements are attached. In the case of a bioaffinity QCM biosensor,[38] it is based upon self-assembling an alkane thiol monolayer with succinyl linkage to different synthetic epitope peptides that are recognition elements for specific viral capsid proteins. These investigators carefully examined a number of conditions necessary to form a densely packed monolayer completely covering the gold surface as assayed by X-ray photoelectron spectroscopy and scanning force microscopy. This biosensor was then used to measure antibody binding that was specific to the immobilized recognition peptide. This biosensor could be regenerated after use.

In the case of mercaptohexylthiol monolayers self-assembled on the gold QCM surface for the purpose of oligonucleotide attachment and subsequent DNA hybridization,[66] these investigators mixed an additional reduceable thiol, mercaptopropionic acid, in with the oligonucleotide derivatized mercaptohexylthiol. Following monolayer formation, they then reduced the mercaptopropionic acid, which caused it to desorb. This increased the efficiency of DNA hybridization in the subsequent step by an order of magnitude compared to self-assembling the pure oligonucleotide derivatized mercaptohexylthiol film, because of the bare gold's

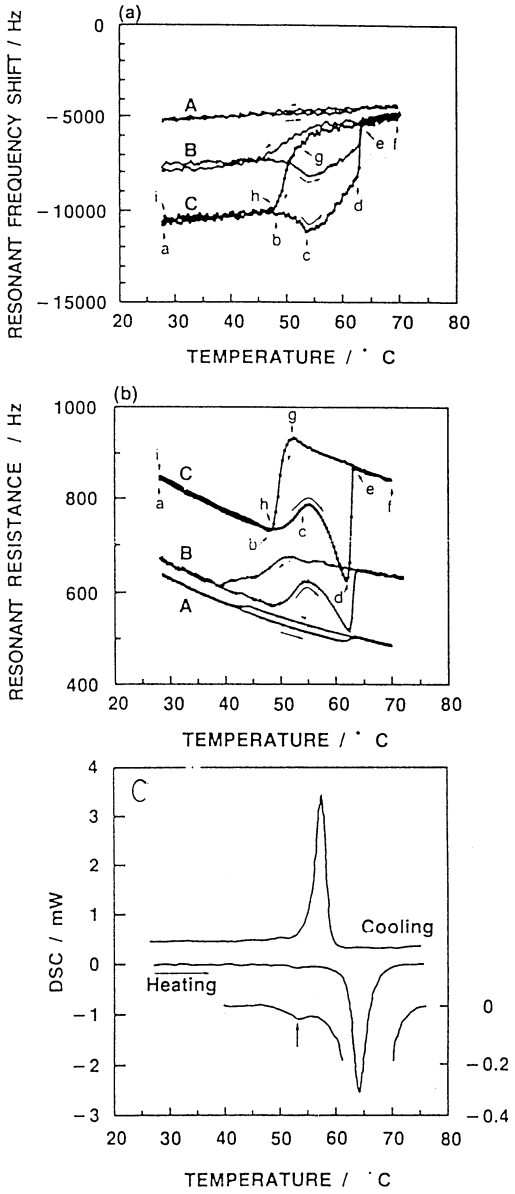

Figure 8. Resonant *f* change with temperature increasing and decreasing in panel a for QCM crystals covered with $2C_{18}OH$ LB films of (A) 10, (B) 30 and (C) 50 layers. Resonant *R* changes with temperature increasing and decreasing in panel b for the QCM crystals coated with $2C_{18}OH$ LB films of (A) 10, (B) 30 and (C) 50 layers. Direction of temperature scan is shown with arrows. In panel c is shown the DSC scans of the same films. The upper arrow shows the first phase transition point on the temperature increasing process. Reprinted with permission from ref 69. Copyright 1992 American Chemical Society.

effect on reducing DNA surface density and promoting a better oligonucleotide orientation for hybridization.

LB films of 1,3-dioctadecyl-rac-glycer-2-ol, exhibiting two thermal phase transitions, were studied as multilayer thin films with the QCM.[69] The *f* and *R* changes measured by these investigators are presented in Figure 8, parts a and b. The first phase transition at the point labeled c, corresponding to the minor transition observed during the heating cycle in Figure 8c, suggested that the film had a small mass increase (*f* decrease) and viscosity increase (*R* increase). The viscosity increase was explained based upon the loss of hydrophobic interactions during the first phase transition. Following the region between phase transitions, labeled c and d in Figure 8, parts a and b, at the second phase transition labeled d, where a major negative peak exists in the heating cycle in Figure 8c, both *f* and *R* increased. This behavior was explained as a loss in film elasticity and a viscosity increase, because of the disappearance of hydrophilic bonds in the film during this second phase transition.

Molecular Imprinted Polymer Film and Chemical Sensors. Historically, the QCM was first applied to create chemical sensors for detection of species in the vapor phase. Although it is not our intent to discuss vapor phase QCM applications in this review, it is worth mentioning that recent reports of vapor phase sensors utilize polymers as the active binding elements for vapor phase molecules. In the case of a humidity sensor, poly(D,L-lactide) and poly(lactide-*co*-glycolide) were used.[70] For certain so-called odor sensors,[71] deposition of polypyrrole films upon the QCM surface acts as the vapor species binding element. Vapor versus solution phase differences aside, these systems resemble the use of the QCM for the recognition of other small molecules in solution based upon immobilized molecular imprinted polymer films as the active recognition species. These solution systems include recognition of small molecules such as terpenes[72] and caffeine[73] as well as large proteins such as lysozyme.[74] An additional feature in some cases is chiral recognition, such as for the amino acids D and L glumatic acid.[75] We discuss more examples where molecularly imprinted polymers have been used for sensitive detection of drug molecules in the section below on Drug Discovery Applications.

Nanoarchitecture and Layer-by-Layer Films. By definition, the careful creation of thin films using the layer-by-layer technique coupled with the molecular design of how succesive layers interact can produce nanoarchitectured multilayer films. The degree of order and functionality in such films remains a key outcome of this approach. The QCM is aptly suited to the study of layer-by-layer deposition of films and a number of such investigations involving biological macromolecules have been carried out. These studies focus on alternating polymer layers with protein[76−84] and DNA[85,86] containing layers. Other investigations contain biopolymers as a part of the layer structure for medical device surface studies.[87,88] We discuss a few of the more interesting reports below.

The formation of electrostatic alternating layers of the polycationic poly(diallyldimethylammonium) (PDDA) and the anionic protein hemoglobin (Hb) at pH 9.2 was studied via EQCM. An appropriate Soret band in the visible region as well as the IR amide band demonstrated that the Hb maintained its native conformation within the multilayer film.[76] The Fe(III)/Fe(II) redox couple of the native Hb in the $[PDDA/Hb]_8$ layer film was then studied via reduction of trichloroacetic acid and nitrite ion as well as oxygen and hydrogen peroxide reactions. In another study, alternating layers of anionic glucose oxidase (GO), lactate oxidase, or soybean peroxidase and redox cationic poly(diallylamine) with covalently attached $[Os(bpy)_2ClPyCOH]^+$ (PAA-Os) were assembled on metal electrode surfaces and studied electrochemically.[81] The enzymes were "wired" to the electrode surface via the PAA-Os redox polymer. Differences

in GO wiring efficiency were detected with different assembly procedures. In related systems, where enzymes were incorporated into alternately charged polymer layers, increased thermal stability of GO and alkaline phosphatase were associated with an increasing number of deposited enzyme layers,[83] and cholesterol oxidase formed a multilayer biosensor.[84] In the latter report, a series of layer-by-layer structures were formed on a variety of solid substrates that were investigated by AFM. The biosensor was used to detect cholesterol over a range of concentrations.

Thin film structures formed from layer-by-layer build-up of alternating humic acid based polymers and ferric ions were investigated as potentially biocompatible multilayer structures for implantable glucose sensors.[79] In this study, a strong pH and ionic strength dependence was observed for the multilayer formation process. From combined QCM and ellipsometry studies, a layer stickness of 24.3 nm was observed. From a functional standpoint, the glucose permeability could be regulated by changing the layer number. Also a 200 nm thick multilayer film was found to have a shear modulus of 80 MPa, suggesting that it would be stable upon implantation. In vivo studies of the multilayers indicated that only a mild inflammatory response occurred along with some neovascularization. Another type of biocompatible film, formed from alternating poly(L-lysine) and hyaluronic acid, a natural cartilage polymer, was studied by streaming potential, AFM, QCM, and optical waveguide lightmode spectroscopy.[88] This study demonstrated that the driving force for multilayer build-up follows two regimes. The first is the formation of isolated islands and their coalescence. The second is the continuous film regime, beginning after the 8 th layer has formed and is characterized by an exponential increase in mass. QCM measurements at different *f* values produced evidence for viscoelastic film behavior, with a measured shear viscosity on the order of 0.1 Pa s.

QCM Application to Studies of Biochemical Processes, Biomimetic Systems, Biosensors, and Drug Discovery

The versatility of the QCM technique has allowed investigators to carry out the following biochemically oriented studies: (1) form and study biomimetic systems; (2) investigate a range of fundamental biochemical processes; (3) create biosensors by immobilizing biochemical components (nucleic acid, protein) or whole cells onto the QCM surface or within a polymeric film on the surface; (4) investigate drug-target interactions for drug discovery applications. Although in many of these applications of the QCM there is clear overlap between the study of basic biochemical processes, biomimetic systems, biosensors, and drug discovery applications, we have attempted to distinguish these application classes in the following discussion.

QCM Investigations of Biomimetic Systems. A number of QCM based investigations have been made of biomimetic systems. We briefly discuss some of the more important of these applications. Biomimetic systems include investigating the properties of protein monolayers on surfaces,[89−94] an artificial tongue that senses the isohumulone and tetraisohumulone components in beer responsible for bitterness,[95] a vapor phase odor sensor[71] and the solution phase molecular imprinted polymer based small molecule sensors[72−75] discussed previously; ion channeling phenomena studied via EQCM in model biomembranes,[96] an antibiotic influencing lipopolysaccharide phase behavior,[97] adsorption of disinfectant by a synthetic multibilayer and correlation with its inhibitory concentration,[98] and a bioadhesion model for the glycocalix, the biological lipid−protein bilayer complexed with cytoskeleton.[99]

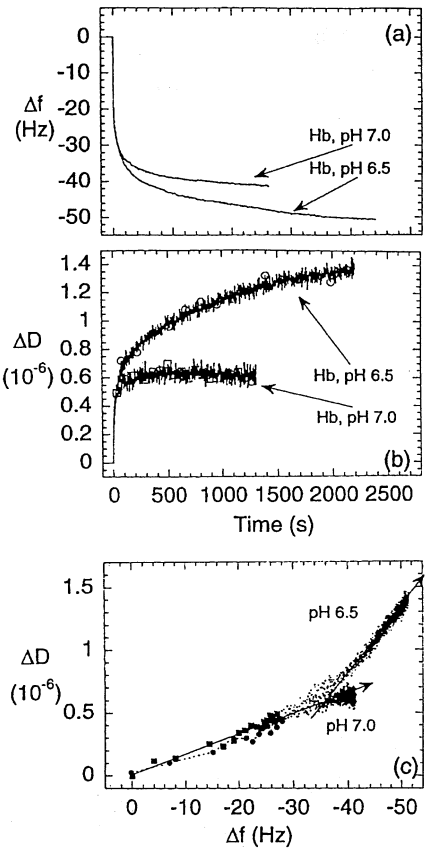

Figure 9. Δf vs time plot in panel a and a ΔD vs time plot in panel b for the adsorption of hemoglobin on a hydrophobic surface at pH 6.5 and 7.0. The influence of pH on hemoglobin adsorption kinetics is illustrated in the $\Delta D-\Delta f$ plot in panel c. Circles are pH 7.0. Squares are pH 6.5. Reprinted with permission from ref 90. Copyright 1998 American Chemical Society.

We describe the results from three of these biomimetic studies that provide detailed views of the systems under study. In the first, the time-resolved adsorption kinetics of four different proteins (myoglobin, hemoglobin, human serum albumin, ferritin, and human serum albumin-antibody) to a methyl terminated alkane thiol modified QCM surface were examined via *f* shifts and *D*-energy dissipation factor measurements.[90] All proteins caused *f* decreases due to formed films and *D*-factor changes revealed that different phases occurred during the adorption process. In Figure 9a−c, measurements of *f* and *D* shifts for hemoglobin adsorption to the hydrophobic surface is presented for two different pH values. At pH 6.5, the Hb mass uptake (Figure 9a) is marginally greater and the energy dissipation (Figure 9b) is considerably greater than at pH 7.0. The graph in Figure 9c demonstrates that the linear behavior at pH 7.0 is replaced by a more complex two phase behavior at pH 6.5.

The second study was of mussel adhesive protein, the foot proteins of *Mytilus edulis* comprised of 75−85 repeats of a

Table 1. Binding and Dissociation Rate Constants (k_1 and k_{-1}) and Association Constants (K_a) of a Target 3′CCCTTAAGCA5′ to a Probe Biotinylated-5′GGGAATTCGT3′ on a QCM at 20 °C[a]

run	instrument	immobilization method	k_1 (10^3 M^{-1} s^{-1})	k_{-1} (10^{-3} s^{-1})	K_a (10^6 M^{-1})
1	27 MHz QCM	avidin-biotin	24	20	1.2
2	BIAcore	avidin-biotin on a bare Au[b]	62	7.4	8.4
3	BIAcore	avidin-biotin in dextran matrix[c]	55	15	3.8

[a] 10 mM Tris, pH 7.8, 0.2 M NaCl, 1 mM EDTA, 20 °C. Each run was examined at least three times and the experimental errors were within ±10%. [b] Biotinylated nucleotide probes were immobilized on an avidin monolayer on a bare Au surface of a sensor tip. [c] Biotinylated nucleotide probes were immobilized on an avidin that is covalently bonded to carboxymethyl groups in a swelled dextran layer.

decapeptide unit. This protein was also studied in detail by the same group on the same self-assembling alkane thiol monolayer mentioned above using three complementary techniques: QCM, SPR, and ellipsometry.[91] Formation of a bioadhesive biomimetic protein film demonstrated that, upon chemical cross-linking, the protein film transformed from a 20 nm, water rich, hydrogellike state to a much thinner compact 5 nm, less water rich film state. Their quantitative data on thickness, shear elastic modulus, and shear viscosity of the film and *f* and *D*-energy dissipation measurements, performed at multiple frequency harmonics of the crystal, were combined with theoretical simulations of the film properties using a Voight based viscoelastic model.

In the third study, an EQCM based experiment, a model membrane biomimetic study of L-α-dipalmitoyl phosphatidyl choline (DPPC) lipid bilayers on gold electrodes modified with a gramicidin ion channel, was carried out.[96] The bilayer film was found to be elastic. When Tl^+ ions were taken up in the gramicidin channels in a chronopiezogravimetric experiment, Tl atoms were measured to be deposited at the electrode surface forming an interlayer. Sharp *f* spikes were associated with uptake, formation, and dissolution of Tl atoms. Mechanistic models of dynamic DPPC bilayer phase changes were evaluated during negative step potentials. Calculations confirmed that the formation of a cylindrical DPPC aggregate phase can result in sufficient water entrapment to account for the measured *f* shifts.

Studies of Fundamental Biochemical Processes—Nucleic Acid Systems. Many types of fundamental biological processes have been studied with the QCM, and in the discussion that follows, we relate the breadth of these studies and examine some in detail. Fundamental molecular processes involving DNA have been the subject of a number of QCM studies. The basic DNA hybridization process has been examined,[60,101,102] and its second-order rate constants were found to be similar to solution values.[103,104] During DNA hybridization, changes in the physicochemical properties of DNA during the reaction time course have been studied,[105−107] as well as during the process of DNA−PNA (peptide nucleic acid) hybrid formation.[108] DNA−drug binding has been investigated via chemical modification of single and double standed DNA with *cis*-Platin,[109,110] binding double stranded DNA with nogalamycin,[111] and via intercalation of drugs such as Hoechst 33258 into the double helix.[102] Interactions between even larger molecular systems, such as RNA−protein and DNA−protein complexes,[111−113] have been studied.

The earliest studies demonstrated that DNA hybridization was detectable via the QCM. More recent investigations have

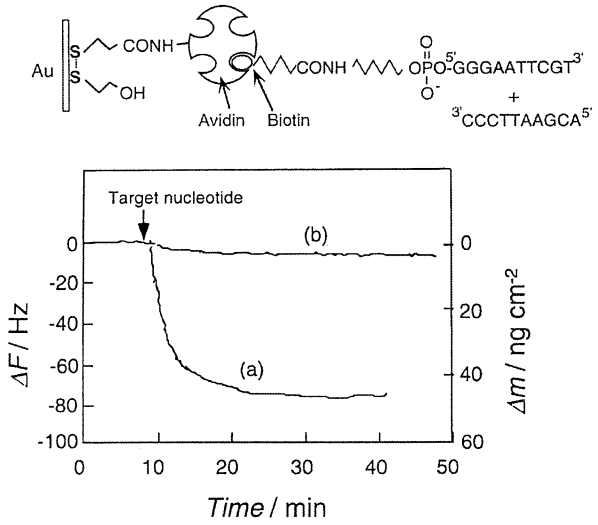

Figure 10. Schematic of DNA hybridization on an oligonucleotide immobilized on a 27 MHz QCM. The time course of *f* decrease for 5′GGGAATTCGT3′ immobilized on the QCM in response (arrow) to (a) a fully complementary 3′CCCTTAAGCA5′ and (b) 3′CCCTGAAGCA5′ having one base mismatch in the middle of the sequence. Figure and Table 1 reprinted with permission from ref 104. Copyright 2000 Japan Society for Analytical Chemistry.

demonstrated a number of important facts. For immobilized denatured *E. coli* DNA of a few hundred base pairs on a nonporous adsorbing QCM surface, a second-order kinetic process was demonstrated for DNA hybridization of a nonspecific target sequence, as is the known case for solution DNA hybridization.[103] Furthermore, the measured rate constant of 2.2×10^{-6} mL μg^{-1} s^{-1} was found to be statistically indistinguishable from the same rate constant measured for hybridization in solution via other techniques.

In another study, short oligonucleotides were hybridized to a QCM gold surface immobilized avidin−biotinylated complementary oligonucleotide and assayed with a sensitive 27 MHz QCM device.[104] The discriminatory capability of this QCM system is illustrated in Figure 10 where the nearly 80 Hz decrease in response to complementary oligonucleotide hybridization can be compared to no *f* change in the presence of an oligonucleotide with just one base mismatch. For the complementary oligonucleotide hybridization, both rate constants, k_1 and k_{-1}, for the process were measured and are compared in Table 1 very favorably to the same parameters measured with the BIAcore Surface Plasmon Resonance instrument.

In a study utilizing an on-line QCM biosensor with continuous flow and stop flow capability, the hybridization of a biotinylated 25-mer oligonucleotide probe with complementary, noncomplementary, and a series of single base

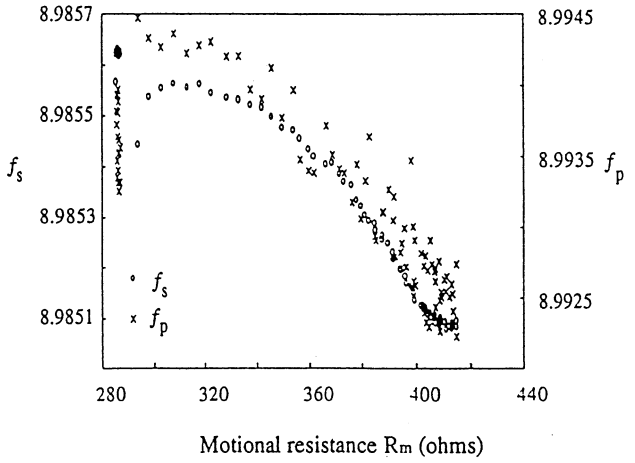

Figure 11. Response of the characteristic f_s and f_p values presented vs the motional resistance R_m upon hybridization of immobilized poly C with poly G in solution at 60 °C. Reprinted with permission from ref 107. Copyright 1996 American Chemical Society.

mutated 25-mer targets was studied after flow was stopped at the QCM surface.[106] Detailed studies of these single base mismatched targets allowed these investigators to distinguish different types of single base mismatches as well as the location of the base mismatch in the 25-mer target. This interesting discriminatory power of the QCM relies on differences in structural features of the different duplexes that are currently not understood.

A liquid-phase acoustic network analysis of DNA and RNA hybridization has been carried out that examines the time course of hybridization of complementary single stranded DNA in solution to single stranded DNA immobilized on the QCM surface.[107] The mass determined to be added to the surface as a result of hybridization was found to compare favorably with scintillation counting of the ^{32}P label contained within the surface bound DNA used in the experiments. Following DNA hybridization, the measured *f* change is 18 times that predicted by the Sauerbray equation for the addition via hybridization of the equivalent mass, as elastic mass, to the QCM surface.[106] This significant difference was ascribed largely to an increase in viscoelastic behavior during hybrid formation. DNA double helices are known to create a significantly higher viscosity solution environment than an equivalent concentration of single stranded DNA mass. For the case of the RNA hybridization process studied by impedance analysis, Figure 11 shows the decrease of f_p and f_s with increasing R_m.[107] These results demonstrate a complex response and an increase in the energy dissipation behavior upon hybrid formation. Certainly, the formation of RNA double helix would be expected to increase R_m, because the bulk solution viscosity has long been known to be higher for relatively rigid double helical nucleic acid compared to an equivalent concentration of flexible single stranded nucleic acid.

For the drug nogalamycin binding to short DNA duplexes immobilized on the QCM surface, the investigators found that 2 nogalamycins were bound to a 12-mer DNA, whereas 7 nogalamycins were bound to a 34-mer DNA.[111] These observations are consistent with the known steric hindrance of nogalamycin to neighboring drug molecules binding to closely spaced 5′TpG and 5′CpG sites in the oligomeric DNAs. Greater energy dissipation effects were measured for the 34-mer compared to the 12-mer DNAs. Even greater energy dissipation was measured for the drug bound 34-mer, which is consistent with a known lengthening effect of the 34-mer as nogalamycin binds.

In another study utilizing an on-line 9 MHz QCM system, the HIV-1 TAR RNA, the transcript of the trans-activation response element at the 5′ end of the HIV-1 viral mRNA transcript, was immobilized on the gold QCM surface and studied interacting with two different Tat derived peptides, 12 and 40 amino acids in length.[112] The native Tat viral protein is 86 amino acids long and binds to a highly conserved TAR RNA sequence 60 nucleotides in length, which includes a stem-loop structure incorporating a three nucleotide bulge. The three nucleotide bulge represents an important recognition and binding site feature for the Tat protein. This study reported series *f* and *R* results for the interaction that indicated a reversible equilibrium for both Tat peptides and determined the k_{off} rates for both TAR RNA−peptide complexes. Removal of the three nucleotide bulge from the TAR RNA resulted in increased off-rates for the Tat peptides. Interestingly, the Tat_{12} peptide exhibited single-exponential dissociation kinetics, whereas the Tat_{40} peptide exhibited biphasic exponential dissociation behavior, in agreement with previous results reported for this system in the literature. Another interesting feature observed in this system was that the initial *f* shifts observed for binding the Tat_{12} and Tat_{40} peptides were of opposite direction. The lower limit of detection of the Tat_{12} peptide in this TAR RNA binding system was estimated to be about 1×10^{-7} M.

A sensitive 27 MHz QCM device was used to help design an asparagine and lysine containing alanine based helical peptide, 16−17 amino acids in length, that selectively bound A−T base pairs in a series of homopolymeric DNA duplexes bound to the crystal surface.[113] The binding isotherms and equilibrium K_{aff} values for these different oligomeric DNA−helical polypeptide complexes were determined and correlated with CD spectra to help understand the best binding complexes for the next step in molecular design.

QCM Studies of Protein and Immunological Systems. Protein systems have been addressed in a number of QCM studies. These include a study of the kinetics of mass deposition and viscoelastic changes accompanying blood clotting.[40,100] In the latter study, QCM with energy dissipation was compared to surface plasmon resonance. These investigators found that surface plasmon resonance detected optical evanescent wave effects earlier in the clotting process, but the QCM detected physical changes in the clot over a longer time frame. Both methods detected dependencies on the concentration of coagulant activator and a sensitivity to heparin addition. The ratio of *D*-energy dissipation factor to *f* shift, reflecting viscoelastic changes in the clot, varied with the coagulant activator concentration in blood plasma but not whole blood. Addition of heparin to whole blood made the dependence reappear. Also in related studies, the QCM was used as a bioassay method for the screening of new biomaterials surfaces.[114,115] The surfaces examined had the following relative ranking in their activity toward the

immunological complement activation process: spin coated polyurethane urea > polystyrene = self-assembled monolayers of hydrophobic C_{18} alkane thiol > sputtered Ti. In these studies, a comparison of QCM to the surface plasmon resonance technique was also made and both showed comparable sensitivities on gold surfaces. However, on the three biomaterials coatings that were polymeric, the SPR method proved problematic because of increased light penetration of the SPR chip.

Enzymatic catalysis has been studied from a basic activity measurement perspective as well as a fundamental mechanistic point of view. As we described previously, horseradish peroxidase activity could be detected via increases in the solution viscoelastic properties produced by the polymer product of the reaction in an optically opaque solution of surfactant monomer (decyl ester of tyrosine) aggregates.[45] Degradative enzymatic activity was also detected via a related approach.[64] However, far more detailed mechanism based studies of enzymatic catalysis have also been performed. For example, polyphenol oxidase, immobilized in a layer-by-layer system with cationic poly(allylamine), has been studied with EQCM and the rate constants determined.[80] This study established that the decomposition rate for the enzyme−substrate complex is slower than the enzymatic reoxidation step.

In a significantly more complex enzymatic system, the interaction and activity parameters of enzymes with immobilized DNA as substrate have been measured.[116,117] In the latter report, the investigators directly monitored the kinetics of DNA polymerase activity upon an immobilized DNA on the surface of a 27 MHz crystal.[117] They found that this sensitive QCM device could allow them to measure the three separate phases of the DNA polymerase reaction: (1) polymerase binding to the primer; (2) elongation via incorporated nucleotides along the template; (3) release of the enzyme from the completely polymerized template. Binding constants and appropriate rate constants, k_f and k_r, were measured for all steps in the process. The repair function of this enzyme could also be measured.

Many examples in a class of important protein−protein interactions have been studied with the QCM. These are the antibody−antigen[118−127] interactions and a related class of interactions, glycoprotein−protein interactions.[128−130] In many of the former class of interactions, the QCM was utilized primarily as a biosensor of an antigen of interest in solution and the detection sensitivity was the primary focus. We discuss this class in the following section on biosensors. In the latter class, glycoprotein−protein interactions, the QCM measured interesting properties of these interactions. As an example, in Figure 12, we consider the 9 MHz QCM equilibrium binding and kinetic study of Concanavalin A (Con A) binding to glycolipid monolayers containing increasing concentrations of $2C_{18}$-mal(alpha-D-glucopyranosyl-D-gluconamide headgroup).[128] Based on a Langmuir adsorption isotherm model, the Con A binding and dissociation rate constants and the affinity constant were calculated for the varying glycolipid compositions from these data and are shown in Table 2. These authors reasonably justify their conversion of *f* shifts to bound mass to determine concentrations and therefore affinity constants from QCM measurements with the following two arguments. First, the *f* shifts because of monolayer film pick-up on the QCM surface, when converted to bound mass, agree with the mass of monolayer molecules known to be found in an area of the Langmuir−Blodgett trough equivalent to the area picked up by the QCM crystal. Second, the affinity constants determined from the QCM experiment agree with independent experimental determinations utilizing radiolabeled Con A binding to similar films. In this study, Con A was shown to exhibit a specificity for lipids possessing the alpha-D-glucopyranosyl-D-gluconamide headgroups. In a different study of a complex binding system, shiga toxins, from *Shigella dysenteriae*, were studied and could be differentiated by applying a monoalkyl globobioside as the toxin ligand.[130]

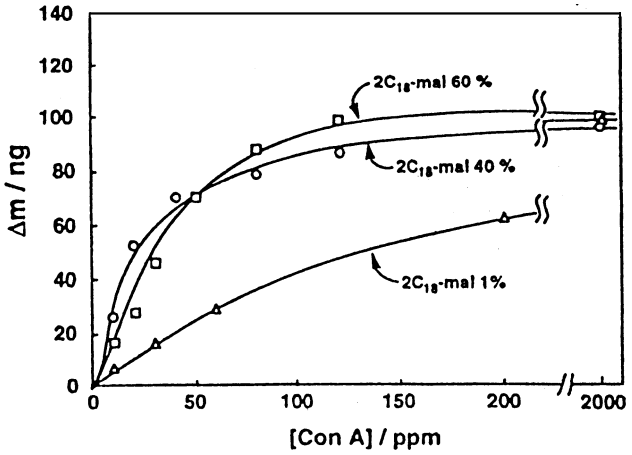

Figure 12. Saturation binding behavior of Con A to the mixed monolayer of $2C_{18}$-mal (1, 40, and 60 mol %) and $2C_{18}$PE as a function of its dependence on the concentration of Con A in the buffered subphase and at a surface pressure of 30 mN. The solid lines represent fits to Langmuir adsorption isotherm behavior. Figure and Table 2 reprinted with permission from ref 128. Copyright 1994 American Chemical Society.

Table 2. Binding (k_1) and Dissociation (k_{-1}) Rate Constants and Association Constants (K_a) of Con A with the Mixed Monolayer of $2C_{18}$-mal and $2C_{18}$PE

monolayer content ($2C_{18}$-mal:$2C_{18}$PE)	k_1 ($M^{-1}\ s^{-1}$)	k_{-1} ($10^{-6}\ s^{-1}$)	$K_a = k_1/k_{-1}$ ($10^6\ M^{-1}$)	K_a [a] ($10^6\ M^{-1}$)
1:99				0.6
5:95	1800	1400	1.3	
20:80	420	170	2.5	
40:60	190	61	3.1	2.8
60:40	250	210	1.2	1.6

The QCM has been applied to studying the interactions of much larger systems than macromolecules or biopolymers. Whole viruses or bacteriophage have been investigated.[131−135] These studies have been carried out utilizing recognition by the native cell surface binding molecule immobilized to the QCM surface in the case of influenza virus binding to monosialoganglioside (GM3);[131] and coat protein antibody immobilization on the QCM surface in the case of M13 phage,[132,133] HSV 1 virus,[134] and orchid viruses.[135] In the case of the influenza A virus, the investigators examined the minimum monosialoganglioside(GM3) membrane concentration necessary for virus binding.[131] For the studies of M13 phage and HSV 1 virus, these investigators have developed

new innovative approaches to applying the QCM. In the case of M13 phage, higher detection sensitivity was achieved by increasing the operating f range.[132] In related studies, another group measured the strength of the M13 phage and HSV 1 virus interactions with immobilized antibodies by a new variant of traditional QCM called rupture event scanning.[133,134] In the final section of this review, concerned with new technological developments, we discuss these reports in more detail.

QCM Studies of Living Cells. Finally, the largest fundamental biological processes studied with the QCM have been those involving living cells. For the most part, these studies have focused on the process of cellular adhesion. In the case of biofilms, the cells are bacterial.[136] Living cells from eukaryotic organisms have been studied on the QCM because their adhesion behavior is an important part of the normal cell phenotype. The cells studied include endothelial cells, osteoblasts, human platelets, MDCK I and II cells, 3T3 cells, VERO cells, CHO, and MKE epithelial cells.[24,33,35,137−148] The earliest studies demonstrated considerable variability in reported frequency shifts, but they all served to establish, perhaps not surprisingly, that cells bound to the QCM surface produced *f* shifts that were reversible upon their removal and that the cells did not behave as elastic masses.

In fact, the inapplicability of the Sauerbray eq 1 to cell attachment was pointedly made in one study.[141] Here, the QCM *f* response produced by binding human platelets was compared to the calculated cell mass bound via measuring a ^{51}Cr radiolabel incorporated into the cells. Using the measured *f* decrease following cell attachment, converted to effective bound mass using the Sauerbray eq 1, these investigators found the value to be 200× less than the actual bound cell mass based on their radiolabeled measurements.

Only a few investigators have used the sensitive quantitative capabilities of the QCM to investigate the behavior of adherent cells in response to chemical, biological, or physical changes in their environment. In particular, the mass and viscoelasticity sensing features of the QCM technique make it attractive for the study of changes in surface adherent cells. As an interesting and detailed example, the early time course of endothelial cell attachment up to their steady-state behavior at 24 h has been followed in a series of studies and correlated with fluoresence light microscopy simulations of the attachment process.[24,33,146−148] These studies have demonstrated the following interesting features. There is a 10 min lag between the appearance of endothelial cells at the QCM surface and the earliest changes in *f* and *R* of the quartz crystal.[33] Therefore, this deliniates the average amount of time necessary for the cell to begin forming surface attachments that provide measurable mass coupling. Following this short lag period, the earliest cell attachment behavior exhibits significant evidence of cell density dependence, or cell−cell cooperativity, in its effect on changes in the QCM *f* and *R* parameters. By contrast, at longer attachment times, around 20 h or more, steady-state cell attachment is exhibited. In this regime, the cell density dependence of the *f* and *R* parameters has changed and no longer exhibits evidence of any cell−cell cooperativity. Early cell attachment also produces the lowest level of energy

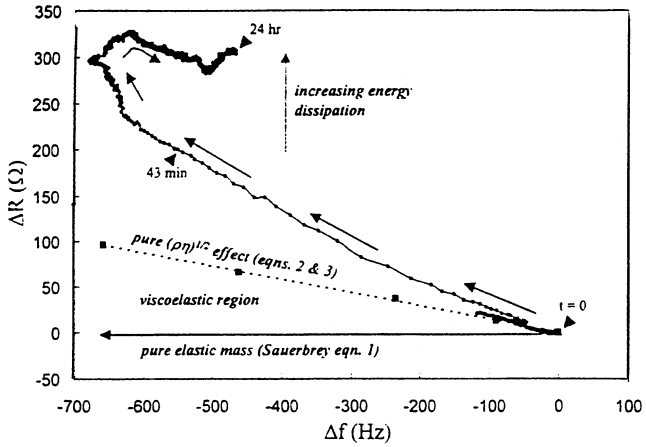

Figure 13. $\Delta f-\Delta R$ diagram representing the time course (arrows) of 30 000 cells added to the QCM at $t = 0$. The pure $(\rho\eta)^{0.5}$ effect line is indicated with the dashed line and some experimental data points (solid squares) for different % sucrose solutions. The horizontal solid line indicates Sauerbray eq 1 behavior for elastic mass binding to the surface. Reprinted with permission from ref 24. Copyright 2000 American Chemical Society.

dissipation, resembling the density−viscosity alterations due to a Newtonian fluid, corresponding to the line labeled CD in Figure 3 and in Figure 7 the dashed line and experimental sucrose calibration points.[24,33] In Figure 13, we present an example of this behavior from the former reference. Here, it is clear that for the first 100 Hz decrease in *f* following cell addition at $t = 0$, the response lies directly on that of the pure liquid $(\rho_L\eta)^{0.5}$ effect line. That is, the cells closely mimic the energy dissipation properties of a liquid. This effect lasts no more than 20 min and is followed by a region of increasingly negative slope leading to higher *R* values and to a limiting steady-state *R* value at 24 h. On a cellular basis, this increase in the level of energy dissipation behavior is consistent with the known formation of a spread cell morphology produced by the internal cytoskeleton linked to the underlying extracellular matrix that the cell synthesizes as it establishes its steady-state attachment. This energy dissipation behavior of the cell population on the QCM surface is consistent with the known energy dissipation behavior of these cells in vivo, where they line the inner surface of blood vessels. In this environment, one of their biological functions is to help dissipate the pulsatile energy associated with blood flow.

Beyond 24 h, the attached endothelial cells could be followed with the QCM as they were activated to divide by administration of fibroblast growth factor. For a stably attached endothelial cell monolayer at 24 h post-addition, steady state *f* and *R* values change as a function of attached cell number and exhibit saturation behavior for both the hydrophilically treated gold surface compared to the untreated gold surface.[33] Going beyond the basic study of endothelial cell attachment just discussed, these investigators established that the attached endothelial cell-QCM acts as a biosensor for studying drug effects disrupting the cytoskeleton in living cells. The microtubule binding and disrupting drug nocodazole, in the nM to μM concentration range, produced a dose dependent f lowering effect.[147] In Figure 14, the formation of the EC QCM biosensor with 20 000 cells (first arrow) is shown achieving a steady state at about

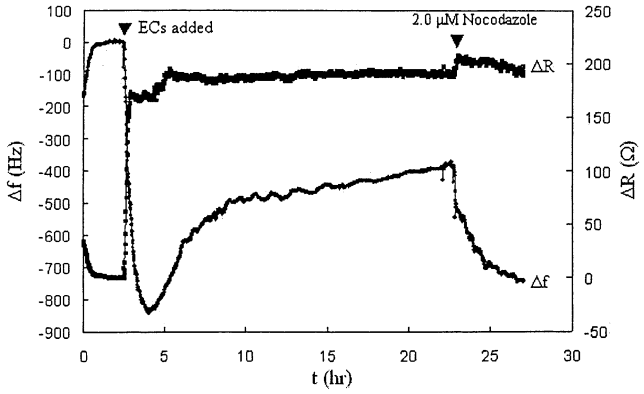

Figure 14. Time dependent behavior of the EC QCM biosensor created by the addition of 20 000 ECs (endothelial cells) at first arrowhead. At the second arrowhead, nocodazole was added to a final 2.0 μM concentration. Reprinted with permission from ref 147. Copyright 2001 Elsevier.

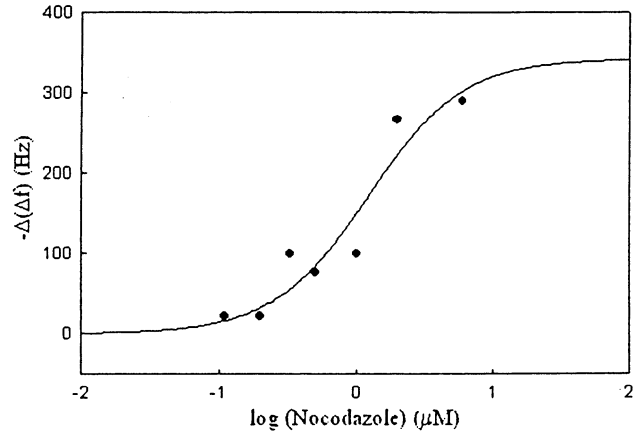

Figure 15. Dose curve of $\Delta(\Delta f)$ as a function of increasing nocodazole concentration where maximum changes in Δf at each dose have been plotted. A three component sigmoid curve has been plotted ($R^2 = 0.91$). Reprinted with permission from ref 147. Copyright 2001 Elsevier.

24 h. This was followed by the administering of 2 μM nocodazole (second arrow), whereupon a nearly 100% f signal decrease was observed, because of microtubule disruption and consequent cell rounding. In Figure 15 is shown a typical sigmoid shaped dose curve of the maximum f decrease achieved by this biosensor over the drug dose range mentioned above. This dose curve covers the range of concentrations where nocodazole has been shown to be effective in the literature references as well as in a parallel tissue culture cell experiment these authors carried out where fluorescence light microscopy verified the QCM dose curve results. These results suggest that, although the cells are initially attached to a nonbiological but not a flat gold surface, the underlying extracellular matrix that they subsequently synthesize and are attached to provides a good approximation to their in vivo cytoskeleton. In a related study, these authors found that the dynamics of the nocodazole dependent microtubule disruption process were fit by a single-exponential decay response, invariant over the nocodazole concentration range.[148] An example of these results are shown in Figure 16 for the 2 μM nocodazole condition. These data strongly indicated the involvement of a single dynamic intracellular system, the microtubules, in the response of the

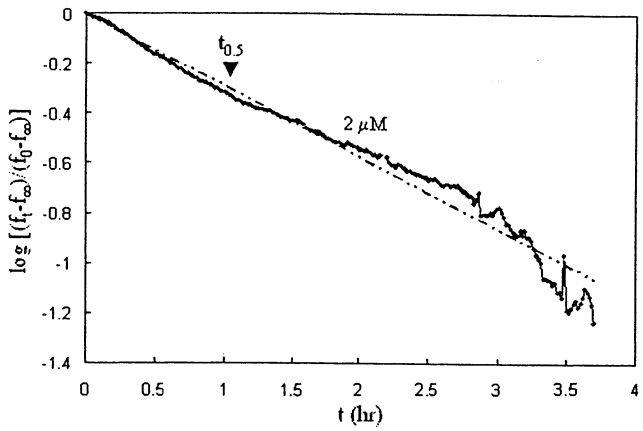

Figure 16. Logarithm of the fraction of remaining Δf change as a function of time due to 2 μM nocodazole addition at the steady state in Figure 14. Linear fit with $R^2 = 0.971$. Reprinted with permission from ref 148. Copyright 2002 Materials Research Society.

attached cells to nocodazole. This cell based QCM biosensor is, in principle, capable of detecting any perturbation in the components of the cellular cytoskeleton and its attachment to the extracellular matrix underlying the cell.

Another group of investigators has taken advantage of the high sensitivity of the central portion of the QCM crystal to record frequency and dissipation factors on low numbers of added cells (hundreds), thereby illustrating the potential sensitivity of this technology.[34,35,143] In addition, the dynamics of exocytosis and dense core vesicle retrieval have been measured in adherent NG 108-15 and PC 12 cells.[144] In a study aimed at understanding the QCM signal magnitudes from attached MDCK-I, MDCK-II, and 3T3 cells,[142,145] an AC impedance analysis (around 5 MHz) was performed in which the measured QCM parameters were modeled as an equivalent circuit. These investigators found that only the mass lying closest to the resonator surface contributed significantly to the signal. They established that the extracellular matrix, cytoskeleton integrity, the distance of the region between cell and underlying substrate, and the mechanical properties of this cleft region all contributed to the QCM signal.

QCM as a Signal Transduction Platform for Biosensors. Many of the studies involving biological macromolecules, and the QCM have been designed not to study the fundamental biochemistry of the biological macromolecules but to exploit their evolved properties for use as the biological recognition elements in biosensors, where they have been integrated with the piezoelectric signal transduction mechanism of this device. All of these biosensor systems require an immobilization step on the QCM surface. In an earlier section of this review, we have discussed a number of reported immobilization strategies where they have been the emphasis of the study, as opposed to the biosensing element integrated with them. However, there are many reports that have appeared, whose emphasis is clearly on the sensing properties of the biosensor being described. In this section, we briefly present an overview of the biosensor applications of the QCM, stressing those literature reports that have focused on practical issues such as biosensor detection sensitivities, reuse, etc.

Immuno- and Enzyme-Based QCM Biosensors. There are a number of major classes of biosensors that involve proteins or peptides and nucleic acids as the recognition elements. Biosensors containing proteins or peptides as the biological elements fall into two groups: immunosensors and enzyme biosensors. The former rely primarily upon the antigen−antibody interaction to carry out molecular recognition and the latter upon the specificity of the immobilized enzyme for a particular substrate.

Immunosensors have been utilized to recognize everything from small molecules to biological macromolecules to whole viruses. QCM immunosensors display a range of detection sensitivities based upon mass binding. They usually demonstrate up to a one 100-fold linear *f* vs mass range and the lower limit sensitivities can be a few μg/mL.[121,123,129] However, in the case of a bacteriophage immunosensor, sensitivities down to as little as 20 bacteriophage were recorded.[133,134] This is due to a novel mechanism of detection called rupture event scanning. In this technique, the energy necessary to rupture the interaction between immobilized antibodies binding bacteriophage is determined by increasing the amplitude of QCM crystal surface oscillation. Then a detector is used to detect the acoustic noise produced when the interaction is broken. For bacteriophage, in the first study, detection is quantitative over 5 orders of magnitude with a lower sensitivity of 20 bacteriophage. In the latter study, HSV-1 virus was sensitively detected in the same way as displayed in Figure 17, parts A and B. These authors claim that the lower limit to the 5 order of magnitude dynamic detection range shown in panel A is in fact 1 HSV-1 virus. For the single virus detection case, panel B shows the rupture event signal magnitude discernible above the background acoustic noise. Because biosensors are studied as potential commercial measurement systems, there are cost concerns. In one study, the focus was on creating a disposable QCM immunosensor capable of detecting human serum albumin in the range from 1 to 250 μg/mL.[123] A peptide immobilized QCM biosensor, using phage display derived peptides, was used as a tissue specific protein biosensor.[149] It was formed on the QCM surface using first a bound biotinylated phospholipid layer, then a streptavidin layer, followed by the biotinylated peptide. This biosensor was capable of detecting tissue specific recognition protein markers in a total protein homogenate of 0.1 mg/mL. Immobilized peptide from murine myofibers produced a significant sensor response only with muscle, but not brain, liver, or kidney tissue homogenates. A similar but lower amplitude response was detected for feline as compared to murine muscle homogenates, indicating species cross reactivity. This type of biosensor may have utility in developing disease diagnostics.

Enzyme biosensors typically utilize an electrochemical reaction of the product species following substrate conversion by the enzyme. Product analyte concentration is measured via the product species' electrochemical oxidation or reduction current at an appropriate potential. Less frequently, enzyme biosensor systems involve the QCM measurement of mass deposition, where the product molecule from the enzymatic reaction is insoluble and precipitates upon the QCM surface.[27,150,26] This leads to interesting measurement possibilities, such as the EQCM based detection of cholera toxin.[27] Here the toxin is first recognized by anti-cholera toxin antibody and then recognition by a horseradish peroxidase functionalized liposome. The enzyme-liposome mediates the oxidation of a substrate, 4-chloronaphthol, to form an insoluble product film on the QCM surface. In Figure 18 is displayed the interfacial electron-transfer resistance or electrode resistance because of the precipitating product film at the electrode as a function of increasing cholera toxin dose. Quantitating this resistance by impedance measurements, coupled with chronopotentiometric and *f* decrease measurements allows these investigators to report an impressive sensitivity detection limit of 1×10^{-13} M for cholera toxin. Enzymatic amplification of the insoluble signal molecule promotes high sensitivity as well as does the combination of measured parameters in this study.

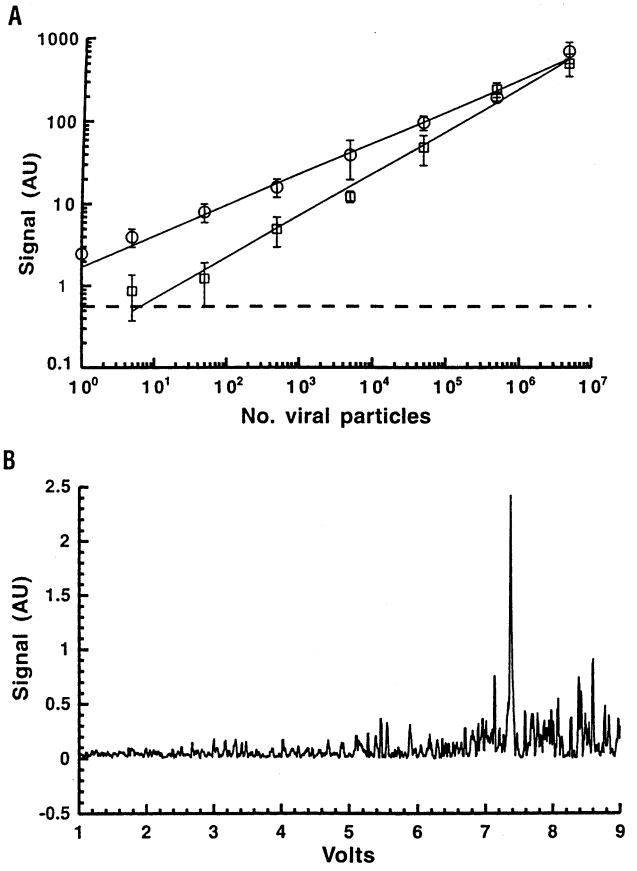

Figure 17. Signal linearity with viral particle numbers. (A) Serial 10-fold dilutions of HSV 1 gD^+ in PBS. A sample volume of either 1 μL (circles) or 40 μL (squares) was incubated for 40 min at room temperature on a QCM surface coated with anti-gD IgG Ab. The dashed line indicates the noise background level. (B) Representative REVS spectrum corresponding to dissociation of a single virion in PBS from an anti-gD IgG mAb-coated QCM surface. The peak can be seen at −7.4 V. Reprinted with permission from ref 134. Copyright 2001 Nature Publishing Group.

Nucleic Acid Based QCM Biosensors. Nucleic acids, primarily DNA in the single stranded form, have been incorporated into a number of QCM based DNA biosensors. The goal is nearly always to measure the extent of complementary single stranded nucleic acid formation resulting from a hybridization step involving the sample to be analyzed. This sequence recognition based quantitation approach can be applied to detect any sequence of interest ranging from

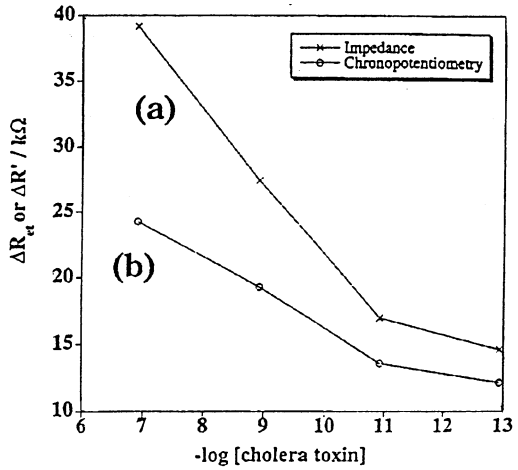

Figure 18. Calibration curves corresponding to the changes in the electron-transfer resistance ΔR_{et} at the electrode (a) or the electrode resistances, ΔR, (b), upon the amplified sensing of different concentrations of the cholera toxin. ΔR_{et} or ΔR corresponds to the difference in electron-transfer resistance after the biocatalyzed precipitation of the converted 4-chloronaphthol substrate or the electron-transfer resistance of the modified electrode before biocatalyzed precipitation of the substrate. Reprinted with permission from ref 27. Copyright 2001 American Chemical Society.

studies in basic biological research to those aimed at biomedical applications such as analyzing clinical samples. The lower detection sensitivities of these biosensors are in the range of a few ng DNA.[102,105,151] Interesting approaches that integrate the molecular recognition hybridization event into the signal transduction pathway of the underlying device have been devised. For example, pyrrole monomers have been chemically linked to single strand oligonucleotides and then electropolymerized with an excess of underivatized pyrrole on an EQCM surface to form a partially derivatized polypyrrole film, which can be used in a subsequent hybridization step.[151] Using both photocurrent spectroscopy measured electrochemically and *f* changes via the quartz crystal (9 MHz), DNA hybridization was detected in the μM range, although this system was not optimized for sensitivity. This DNA biosensor was demonstrated to be reusable for repeated hybridizations.

Recently, a novel DNA biosensor containing a significant mass amplification step has been described.[152] In this system, a thiolated probe oligonucleotide is immobilized on the gold QCM surface (9 MHz), and hybridization to the target analyte is then performed. This is followed by a subsequent hybridization step involving oligonucleotide derivatized liposomes, where the hybridization involves a different sequence region on the target than was used in the first hybridization to the gold QCM surface. A similar approach was also described in this same reference involving biotin-streptavidin modified liposomes that allows build up of liposomes on a single hybridized biotinylated oligonucleotide target. These approaches lead to a significantly higher detection sensitivity of target oligonucleotide: 1×10^{-13} M.

Cell Based QCM Biosensors. QCM biosensors containing whole cells as the active sensing element have also been developed. This is a less intensely studied area than QCM biosensors involving isolated biological macromolecules. This probably results from the added difficulties involved in adapting the QCM for use with living cells where the sterile technique is required, as well as the unfamiliarity of most QCM user labs with cell culture techniques. A requirement for creating such biosensors is that the cells be adherent to the QCM surface. Attachment to an underlying surface is an intrinsic trait of many normal eukaryotic cells. They carry out this attachment via their internal cytoskeleton linking to the extracellular matrix of proteins that they actively create underneath them during attachment. Normal cells that fail to attach to surfaces typically face the initiation of an apoptotic program that results in cell death. Thus, normal cells do not necessarily require an experimentally designed strategy for their attachment. What cells require is a sufficiently hydrophilic surface upon which to initiate the attachment process.[153−155] Thus, a typical gold QCM surface, which is moderately hydrophobic, is not optimal for cell attachment and growth and can lead to variable results. Chemical approaches to increase the hydrophilic character of the surface to promote reproducible cell attachment have been successful.[33] Other modifications of the surface to promote cell attachment have also been demonstrated to be effective. For example, in cell attachment studies, the QCM surface was modified with polystyrene, which was subsequently treated with a UV/O_3 protocol to render it hydrophilic.[143]

As we have discussed in a previous section, many of the published reports studying cells simply demonstrated that they could be grown on a QCM device surface and produced a *f* decrease that was far smaller than was consistent with a bound elastic mass the size of the cell. A few studies have demonstrated the relationship between the magnitude of the *f* decrease and the number of attached cells, rather than the numbers added to the QCM device.[24,33,142] In the first two references, the authors demonstrated that the entire *f* decrease could be accounted for by trypsinization of the cells and their underlying matrix from the QCM surface, returning *f* to its original value. Cell trypsinization from surfaces for transfer is a standard cell biology techique and is considered diagnostic for demonstrating cell attachment. Only a few reports have appeared in which whole cell QCM biosensors have been created and used to detect or sense interesting properties or molecules. As we mentioned in a previous section, in one study, nocodazole, a microtubule binding and disrupting drug, was detected in the nM−μM range, with an endothelial cell QCM biosensor containing only 20 000 added cells.[147,148] Also, fibroblast growth factor activity was detected at 3 ng/mL by its stimulation of attached endothelial cells to divide and decrease *f* over a 72 h period following administration.[24]

In addition to mammalian cell QCM biosensors, biofilms, comprised of prokaryotic bacteria contained within their own synthesized extracellular matrix, have been created on QCM surfaces. Both fimbrilated and nonfimbrilated *E. coli* films were studied interacting with surfaces of varying hydrophobicity as a function of different ionic strengths.[136] Clear differences were detected in *f* and energy dissipation effects between the fimbrilated and nonfimbrilated cells. Only small shifts were detected for fimbrilated cells, but large changes were exhibited by nonfimbrilated cells. Both cell types were

observed to undergo long term changes in these measured parameters, as a result of the establishment of closer contacts between the biofilm and the surface with time. In another study, biofilm formation by *Bacillus coagulans*, *Burkholderia cepacia*, and *Staphylococcus warneri* on the QCM surface were studied as a function of different flow and nutrient conditions.[156] Changes in *f* and admittance were detected over 70 h, and surface cavities on the micron scale were found to serve as low shear environments for bacterial attachment and biofilm formation.

Finally, it should be mentioned that bacterial growth has been detected with novel QCM sensing approaches.[157,158] In the former study, the bacteria were not attached to the QCM, but their growth rate was detected via metabolic acidification of the solution. This caused a normally soluble amphoteric polymer to become progressively insoluble as the solution pH was lowered and the pendant carboxylic acid groups on the polymer became protonated. The insoluble polymer caused the *f* to decrease in a characteristic way that resulted in a cell growth calibration curve. This is not a biosensor as such, but it is a sensor of cell growth. In the latter study, production of ammonia via growth of the urease secreting *Proteus* bacteria was detected using a QCM sensor containing a Teflon barrier that allowed ammonia diffusion into an internal electrolyte solution whose subsequent conductivity alteration caused a decrease in crystal *f*. These authors used this sensor to detect the growth inhibitory effects of antimicrobial polyphenols and catechins found naturally in various green and black teas.[158]

Drug Discovery Applications of QCM. The QCM has been used in a number of studies to test for the presence of drugs over a range of concentrations. This application area, including an evaluation of how QCM could be adapted for drug discovery in the pharmaceutical industry, has been the subject of a recent comprehensive review article.[9] Therefore, we only briefly address this area in the current review. In buffered solutions and other solvents, drugs such as dansylphenylalanine,[159] sialic acid,[160] D and L-phenylalanine,[161] caffeine,[162] procaniamide,[60] trimethoprim,[163] and 5-propranolol[164] have been detected at concentrations ranging from nM to mM. Moreover, drugs such as paracetamol,[165] phenacetin,[166] and *o*-phenylenediammine[167] have also been detected in either serum or urine in the nM to μM range. Many of the most sensitive drug detection strategies employed in the studies referenced above involve recognition by molecularly imprinted polymers immobilized on the QCM surface. Furthermore, in the case of the detection of cefoperazone, a swellable polymeric coating was used that increased the sensitivity by an order of magnitude.[168]

In the case of the whole cell biosensor discussed previously, the drug nocodazole was detected into the nM concentration range, via its effecting a 100% *f* change due to binding and dissociating the microtubule structures within attached endothelial cells.[147,148] The use of this whole cell biosensor for drug detection is a very promising approach because it detected the magnitude and kinetics of a whole cell biological response. This is much closer to the type of information pharmaceutical companies require as drug testing output than is currently available from the high throughput screening done on single macromolecular targets, such as receptors, enzymes, etc. Thus, this cell based approach also allows for the use of mutant or drug resistant cells in the biosensor. This allows one to design strategies for drug target validation or drug rescue kinds of studies in a whole cell environment.

In addition to the pure sensitivity issues required in adapting the QCM for drug discovery assays, a number of other issues become important. These include a surface chemistry requirement for the technique and the current lack of a high throughput capability. Relative to other highly engineered techniques that have been placed in widespread use for drug testing, such as fluorescent labels in a 384 well plate robotic reader format, the QCM is only in its infancy as far as development for the demanding drug application area. However, continued development is warranted because the QCM has advantages over more complex instrumental techniques such as mass spectrometry, DSC calorimetry, and optical techniques such as surface plasmon resonance. These include low cost, label free breadth of applicability, and sensing unique mass distribution and viscoelastic behavior aspects of whole cell responses.

Technology Advances and Future Applications

A number of technology developments promise to advance the applications of QCM and related piezoelectric devices. These development areas include utilizing higher *f* crystals that are significantly more mass sensitive, increasing the effective surface area of the device, utilizing the piezoelectric mechanism in novel ways, and creating higher throughput multiwell devices for commercial applications.

Mass sensitivity has been shown to increase with increasing *f* of crystal oscillation (30 MHz) using thinner milled crystals.[169] Building upon this observation, a recent report described the development of even higher *f* crystals and oscillator circuits to monitor them.[132] Although we have discussed a few reports in which 19−30 MHz *f* crystals were used, they represent the exception rather than the rule to the QCM systems in wide use. In the aforementioned reference, these investigators go well beyond this range. They have created crystals operating in the 39−110 MHz range, the highest reported to date. These higher oscillating *f* crystals were created using chemical milling in the crystal center. This produced thinner, more sensitive, but also significantly more fragile crystals. In this study, they showed empirically that the resonant *f* and mass change relationship for quartz crystals (f^2 factor described in eq 1) has in fact a larger exponent of 2.88. Experimental data from which this exponent was derived is shown in Figure 19A, as the *f* decreases for a given condition of M13 phage binding to surface immobilized coat protein antibodies. There is a dramatic increase in sensitivity going from a crystal oscillation of 19−70 MHz. Practically speaking, this resulted in a 200-fold improvement in detection sensitivity for M13 phage binding to the 56 MHz crystals compared to the same system on 19 MHz crystals. Then, complete M13 phage binding isotherms are presented in panel B for the 19−70 MHz crystal oscillation range. However, the improved sensitivity notwithstanding, at these higher crystal *f* values,

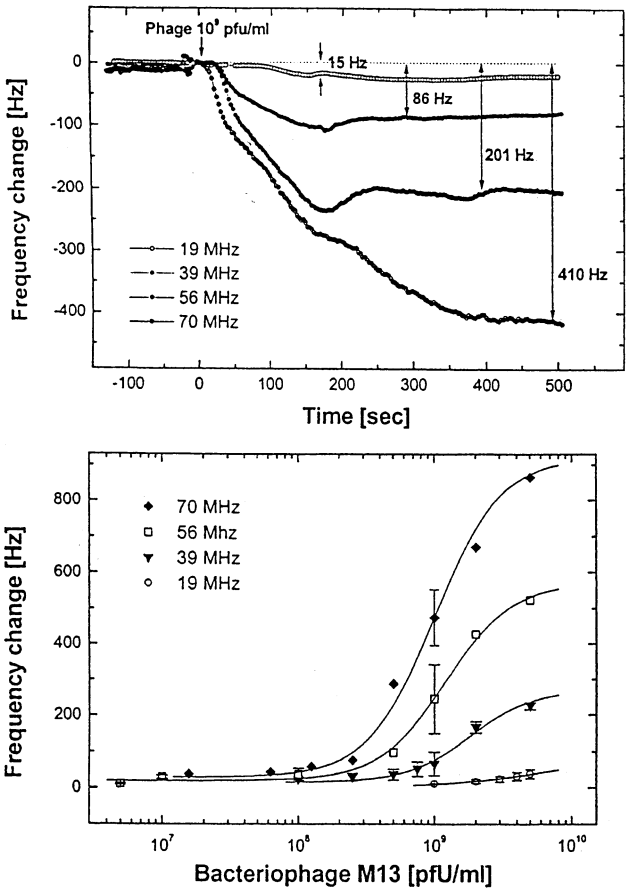

Figure 19. Time response of QCM sensors with different operating *f* values upon injection of M13 bacteriophage (10^9 pfu/mL) in upper panel. In the lower panel are presented dose curves for the detection of the M13 bacteriophage in PBS buffer for the different operating *f* QCM sensors used. Sigmoid curve fits are presented for each operating *f* QCM condition and representative error limits are presented for a few points. Reprinted with permission from ref 132. Copyright 2001 Elsevier.

the conclusion from this interesting study was that overall the practical limit for most uses of QCM lies at around 19 MHz, for which commercial devices exist. At higher frequencies, investigators must build their own oscillator circuits, and at the high end, liquid properties can begin to affect the results.[170] However, the needs of particular application areas, such as in drug discovery, could drive the development of oscillator circuits as off the shelf commercial products. This would place the high *f* QCM crystal techniques within the budget range and technical constraints of most academic and industrial users.

We have already described the novel QCM technology development called rupture event scanning.[133,134] In this technique, viruses (herpes simplex virus 1, M13 bacteriophage) are first bound to antibodies recognizing their coat proteins that have been previously immobilized on the surface of a 14.3 MHz quartz crystal. Then the acoustic energy necessary to rupture the bond is determined. Although this technique covers a wide dynamic range and the detection sensitivity approaches that of single HSV 1 virus particle, a practical limitation of this technology is that only large structures such as viruses, but not proteins, will have sufficient inertial mass to be dissociated from the QCM surface with increasing oscillation amplitude. A device based upon this technique is currently under commercial development to be a compact portable biosensor.

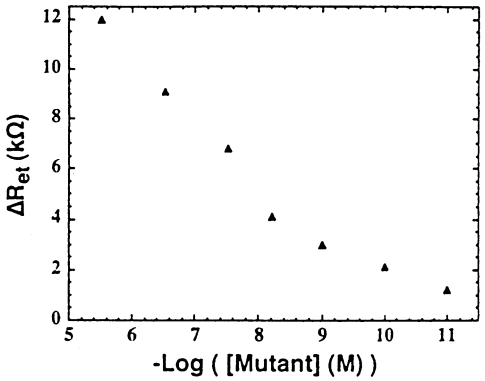

Figure 20. Calibration dose curve corresponding to changes in the electron-transfer resistances of the electrode as a result of the precipitation of alkaline phosphatase catalyzed substrate to an insoluble product at different levels following detection of different concentrations of the 41 base mutant DNA sequence for the Tay Sachs genetic condition. Figure and Table 3 reprinted with permission from ref 174. Copyright 2001 Nature Publishing Group.

Surface enhancement of the electrode deposited on the quartz crystal is another active area of technology development to improve QCM sensitivity. In some approaches, the surface area is being effectively increased via deposition of porous gold electrodes electrochemically or chemical linkage of gold microparticles.[171,172] These modifications have resulted in 3-fold enhancements, respectively, in the protein assay and DNA hybridization assay results found in these two studies. Surface modification via laser micromachining has also been shown to yield a significant (>2.5) enhancement of the signal response in a given system.[173] We have also previously described mass amplifications strategies, including ones where an insoluble precipitate forms on the QCM electrode. One recent study illustrates the application of this concept to the QCM in a system designed to measure hybridization of normal or mutated DNA to an immobilized oligonucleotide.[174] In Figure 20, we show for this system the interfacial electron-transfer resistance ΔR_{et} as a function of the DNA concentration. The specific detection of mutants, but not normal DNA sequences, results from the mutants specific molecular recognition and binding of biotinylated-dCTP, followed by binding of an avidin−alkaline phosphatase complex. Alkaline phosphatase then carries out the enzymatic conversion of 5-bromo-4-chloro-3-indoyl phosphate to an insoluble indigo derivative, which precipitates on the QCM surface bringing about the ΔR_{et} increase. This system yielded a lower sensitivity limit of 1×10^{-11} M DNA. Table 3 illustrates the power and the specificity of this system to not only discriminate the mutant from normal but also to discriminate the homozygous from the heterozygous genetic case where the mutation is in a DNA sequence responsible for the Tay-Sachs genetic condition.

It is worth remembering and re-emphasizing the limitations that variations in interfacial parameters, such as surface roughness, surface free energy, surface charge, and viscoelasticity, place upon the interpretation of QCM results. This is a point that has been emphasized elsewhere.[9] As we discussed earlier in this review, these issues confound the interpretation of *f* shifts in terms of changes in surface mass.

Table 3. Change in the Interfacial Electron Transfer Resistance (ΔR_{et}) upon the Detection of (8) and (a)

sample	reaction with biotinylated dUTP (ΔR_{et}, kΩ)	reaction with biotinylated dCTP (ΔR_{et}, kΩ)
(I) heterozygote (**8**)	1.8 ± 0.1	1.6 ± 0.1
(II) homozygote (**8**)	2.3 ± 0.1	<0.1
(III) normal (**8a**)	<0.1	2.1 ± 0.1

[a] Sequences are as follows: (**8**) ....3′-GAGACGGGGGACCATGGACT-TGGCATATAG**A**TAGGATTAC-5′... (**8a**) ....3′-GAGACGGGGGACCATG-GACTTGGCATATAG**G**ATACCGGG-5′.... (**9**) 5′-HS$(CH_2)_6$CTCTGCCCC-CTGGTACCTGAACCGTATATC-3′.

It is clear from some of the literature references we have discussed, such as living cells on the QCM surface, that f decreases in no way reflect the real mass attached to the QCM surface. On the other hand, some of the literature references studying simpler biomolecular systems showed rough agreement between QCM measured quantities such as equilibrium constants and the same quantity studied by an independent quantitative method. Clearly, there is a considerable range of observed responses when attempting to quantitatively study different systems using the QCM. It must always be kept in mind that the justification to utilize QCM measurements for conversion to mass quantities/concentrations is not something that can be assumed but rather must be demonstrated as feasible on a case by case basis. In the future, it would be desirable to have a clear set of experimentally derived principles or a theory concerning these interfacial variables and their effect on QCM parameters to guide the experimentalist in the design of any experiment and its interpretation.

Most of the QCM experiments carried out currently and referenced in this review have been performed in single well devices. Although there is currently an 8 crystal QCM device sold commercially by Elchema, it is limited to just measurement of f changes.[23] We are likely to soon witness the development of much larger array, multiwell format devices, perhaps utilizing FIA for automated sample injection for use in low throughput screening types of applications in the drug industry.

Finally, it should be mentioned that the widespread quartz based QCM devices we have focused upon in this review are not the only sensing devices that have been developed utilizing piezoelectric transducing materials. It was not the purpose of this review to describe these variants of piezoelectric effect devices, such as surface acoustic wave, flexural plate wave, and acoustic plate mode, which are thoroughly discussed elsewhere.[7,9,175] However, these variants possess some distinct advantages. Some are more sensitive than the QCM, and they are amenable to MEMS microfabrication techniques that could easily result in large array formats. As a sensitivity example, using a two step mass amplification process involving antibody conjugated 40 nm Au particles in the first step and Ag metallization of the gold particles in the final step, a breast cancer antigen was detected in a displacement assay using a flexural plate wave sensor.[175,176] This biosensor system equalled or exceeded the sensitivity of radiolabeled antibodies, detecting the antigen down to the 10^{-15} M range. Continuing development of applications such as these suggest that, in the future, some of the more sensitive piezoelectric device modes will likely be adopted for wide use in the study of systems that QCM is now being applied to, as we've described in this review.

Acknowledgment. The author gratefully acknowledges previous discussions with his collaborators Dr. Tiean Zhou and Dr. Susan Braunhut on certain topic areas contained in this review that were helpful in this writing. Also, NIH grant R21 GM58583 and funding from a Chancellor's Grant at UML are gratefully acknowledged.

References and Notes

(1) Inglese, J. *Drug Discovery Today: High Throughput Technol. Suppl.* **2002**, *7*, S105−S106.
(2) Ilag, L. L.; Hg, J. H.; Beste, G.; Henning, S. W. *Drug Discovery Today: High Throughput Technol. Suppl.* **2002**, *7*, S136−S142.
(3) Huels, C.; Muellner, S.; Meyer, H. E.; Cahill, D. J. *Drug Discovery Today: High Throughput Technol. Suppl.* **2002**, *7*, S119−S124.
(4) Arnold, F. H. *Nature* **2001**, *11*, 253−257.
(5) Ward, M. D. In *Physical Electrochemistry: Principles, Methods & Applications*; Rubenstein, I., Ed.; Marcel Dekker: New York, 1995; pp 293−338.
(6) O'Sullivan, C. K.; Guilbault, G. G. *Biosens. Bioelectron.* **1999**, *14*, 663−670.
(7) Janshoff, A.; Galla, H. J.; Steinem, C. *Angew. Chem., Int. Ed.* **2000**, *39*, 4004−4032.
(8) Wegener, J.; Janshoff, A.; Steinem, C. *Cell Biochem. Biophys.* **2001**, *34*, 121−151.
(9) Cavic, B. A.; Hayward, G. I.; Thompson, M. *Analyst* **1999**, *124*, 1405−1420.
(10) Pavey, K. D. *Expert Rev. Mol. Diag.* **2002**, *2*, 173−186.
(11) Curie, J.; Curie, P. *Comput. Rend. Acad. Sci. Paris* **1880**, *91*, 294−297.
(12) Rayleigh. L. *Proc. London Math Soc.* **1889**, *20*, 225−226.
(13) Cady, W. G. *Phys. Rev.* **1921**, *17*, 531−533.
(14) Lack, F. R.; Willard, G. W.; Fair, I. E. *Bell Syst. Technol.* **1934**, *13*, 453−455.
(15) Sauerbray, G. *Z. Phys.* **1959**, *155*, 206−222.
(16) King, W. H., Jr. *Anal. Chem.* **1964**, *36*, 1735−1741.
(17) Guilbault, G. G. *Anal. Chem.* **1983**, *55*, 1682−1684.
(18) Guilbault, G. G.; Jordan, J. *CRC Rev.* **1988**, *19*, 1−28.
(19) Konash, P. L.; Bastiaans, G. J. *Anal. Chem.* **1980**, *52*, 1929−1935.
(20) Nomura, T.; Okuhara, M. *Anal. Chim. Acta* **1982**, *142*, 281−284.
(21) Kurosawa, K.; Tawara, E.; Kamo, N.; Kobatake, Y. *Anal. Chim. Acta* **1990**, *230*, 41−49.
(22) Kosslinger, C.; Uttenthaler, S.; Drost, F.; Aberl, H.; Wolf, G.; Brink, A.; Stanglmaier, E.; Sackmann, E. *Sens. Actuators, B* **1995**, *107*, 24−25.
(23) http://chemintserver.ucc.ie/sensors/universal/P_PZ1001.htm www.q-sense.com/qsense.htm and www.princetonappliedresearch.com/applications/applicationnotes.htm
(24) Zhou, T.; Marx, K. A.; Warren, M.; Schulz, H.; Braunhut, S. J. *Biotechnol. Prog.* **2000**, *16*, 268−277.
(25) Tanaka, M.; Mochizucki, A.; Motomura, T.; Shimura, K.; Onishi, M.; Okahata, Y. *Colloids Surf. A* **2001**, *193*, 145−152.
(26) Reddy, S. M.; Jones, J. P.; Lewis, T. J.; Vadgama, P. M. *Anal. Chim. Acta* **1998**, *363*, 203−213.
(27) Alfonta, L.; Willner, I.; Throckmorton, D. J.; Singh, A. K. *Anal. Chem.* **2001**, *73*, 5287−5295.
(28) Kanazawa, K. K.; Gordon, G. *Anal. Chim. Acta* **1985**, *175*, 99−105.
(29) Muramatsu, H.; Tamiya, E.; Karube, I. *Anal. Chem.* **1988**, *60*, 2142−2150.
(30) Muramatsu, H.; Egawa, A.; Ataka, T. *J. Electroanal. Chem.* **1995**, *388*, 89−92.
(31) Aberl, F.; Wolf, H.; Kosslinger, C.; Drost, S.; Woias, P.; Koch, S. *Sens. Actuators, B* **1994**, *18−19*, 271−275.
(32) Uttenthaler, E.; Kosslinger, C. *Anal. Chim. Acta* **1998**, *362*, 91−100.
(33) Marx, K. A.; Zhou, T.; Warren, M.; Braunhut, S. J. *Biotechnol. Prog.* **2003**, *19*, 987−999.
(34) Rodahl, M.; Hook, F.; Krozer, A.; Brzenzinski, P.; Kasemo, B. *Rev. Sci. Instrum.* **1995**, *66*, 3924−3930.
(35) Fredriksson, C.; Kihlman, S.; Rodahl, M.; Kasemo, B. *Langmuir* **1998**, *14*, 248−251.

(36) Van-Dyke, K. S. *Phys. Rev.* **1925**, *25*, 895−898.
(37) Schroder, J.; Borngraber, R.; Lucklum, R.; Hauptmann, P. *Rev. Sci. Instrum.* **2001**, *72*, 2750−2755.
(38) Rickert, J.; Weiss, T.; Krass, W.; Jung, G.; Gopel. W. *Biosens. Bioelectron.* **1996**, *11*, 591−598.
(39) Reddy, S. M.; Jones, J. P.; Lewis, T. J. *Faraday Discuss.* **1997**, *107*, 177−196.
(40) Si, S. H.; Zhou, T.; Liu, D.; Nie, L.; Yao, S. *Anal. Lett.* **1994**, *27*, 2027−2037.
(41) Wang, J.; Jiang, M.; Lu, F. *J. Electroanal. Chem*. **1998**, *444*, 127−133.
(42) Koh, W.; DuBois, D.; Kutner, W.; Jones, M. T.; Kadish, K. M. *J. Phys. Chem*. **1992**, *96*, 4163−4168.
(43) Takada, K.; Diaz, D. J.; Abruna, H. D.; Cuadrado, I.; Casado, C.; Alonso, B.; Moran, M.; Losada, J. *J. Am. Chem. Soc*. **1997**, *119*, 10763−10768.
(44) Tanguy, J.; Deniau, G.; Zalczer, G.; Lecayon, G. *J. Electroanal. Chem*. **1996**, *417*, 175−184.
(45) Marx, K. A.; Zhou, T.; Sarma, R. *Biotechnol. Prog*. **1999**, *15*, 522−528.
(46) Long, D. D.; Marx, K. A.; Zhou, T. *J. Electroanal. Chem*. **2001**, *501*, 107−113.
(47) Marx, K. A.; Zhou, T. *J. Electroanal. Chem.* **2002**, *521*, 53−60.
(48) Baker, C. K.; Reynolds, J. R. *J. Electroanal. Chem*. **1988**, *251*, 307−312.
(49) Muramatsu, H.; Ye, X.; Suda, M.; Sakuhara, T.; Ataka, T. *J. Electroanal. Chem.* **1992**, *322*, 311−323.
(50) Lasalle, N.; Roget, A.; Livache, T.; Mailley. P.; Vieil, E. *Talanta* **2001**, *55*, 993−1004.
(51) Bidan, G.; Billon, M.; Galasso, K.; Livache, T.; Mathis, G.; Roget, A.; Torres-Rodriguez, L.; Vieil, E. *Appl. Biochem. Biotechnol*. **2000**, *89*, 183−193.
(52) Wang, J.; Jiang, M. *Langmuir* **2000**, *16*, 2269−2274.
(53) Tjarnhage, T.; Sharp, M. *Electrochim. Acta* **1994**, *39*, 623−629.
(54) Varineau, P. T.; Buttry, D. A. *J. Phys. Chem.* **1987**, *91*, 1292−1298.
(55) Sato, Y.; Mizutani, K.; Shimazu, S.; Ye, S.; Uoski, K. *J. Electroanal. Chem*. **1997**, *433*, 115−123.
(56) Sarma, R.; Alva, K. S.; Marx, K. A.; Tripathy, S. K.; Akkara, J. A.; Kaplan, D. L. *Mater. Sci. Eng. C* **1996**, *4*, 189−192.
(57) Marx, K. A.; Alva, K. S.; Sarma, R. *Mater. Sci. Eng. C* **2000**, *11*, 155−163.
(58) Stalgren, J. J. R.; Claesson, P. M.; Warnheim, T. *Adv. Colloid Interface Sci*. **2001**, *89*−*90*, 383−394.
(59) Njue, C. K.; Rusling, J. F. *J. Am. Chem. Soc.* **2000**, *122*, 6459−6463.
(60) Johnsson, M.; Bergstrand, N.; Edwards, K.; Stalgren, J. J. R. *Langmuir* **2001**, *17*, 3902−3911.
(61) Niwa, M.; Morikawa, M.; Higashi, N. *Kobunshi Ronbunshu* **2000**, *57*, 652−658.
(62) Donohue, J. J.; Buttry, D. A. *Langmuir* **1989**, *5*, 671−678.
(63) DeLong, H. C.; Donohue, J. J.; Buttry, D. A. *Langmuir* **1991**, *7*, 2196−2202.
(64) Krause, S.; Sumner, C. International Patent Application filed, 2000.
(65) Shen, D.; Huang, M.; Chow, L. M.; Yang, M. *Sens. Actuators, B* **2001**, *77*, 664−670.
(66) Satjapipat, M.; Sanedrin, R.; Zhou, F. *Langmuir* **2001**, *17*, 7637−7644.
(67) Tsuchida, A.; Matsuura, K.; Kobayshi, K. *Macromol. Chem. Phys.* **2000**, *201*, 2245−2250.
(68) Nordyke, L.; Buttry, D. A. *Langmuir* **1991**, *7*, 380−388.
(69) Muramatsu, H.; Kimura, K. *Anal. Chem*. **1992**, *64*, 2502−2507.
(70) Sharp, J. S.; Forrest, J. A.; Jones, R. A. L. *Macromolecules* **2001**, *34*, 8752−8760.
(71) Cui, L.; Swann, M.; Glidle, A.; Barker, J.; Cooper, J. M. *Sens. Actuators, B* **2000**, *66*, 94−97.
(72) Percival, C. J.; Stanley, S.; Galle, M.; Braithwaite, A.; Newton, M. I.; McHale, G.; Hayes, W. *Anal. Chem*. **2001**, *73*, 4225−4228.
(73) Kobayashi, T.; Murawaki, Y.; Reddy, P. S.; Abe, M.; Fujii, N. *Anal. Chim. Acta* **2001**, *435*, 141−149.
(74) Hirayami, K.; Sakai, Y.; Kameoka, K. *J. Appl. Polym. Sci*. **2001**, *81*, 3378−3387.
(75) Deore, B.; Chen, Z.; Nagaoka, T. *Anal. Chem.* **2000**, *72*, 3989−3994.
(76) He, P.; Hu, N.; Zhou, G. *Biomacromolecules* **2001**, *3*, 139−146.
(77) Ariga, K.; Sasaki, Y.; Horiguchi, H.; Horiuchi, N.; Kikuchi, J. *Diffus. Defect Data A* **2001**, *191*, 35−59.
(78) Nonogaki, T.; Xu, S.; Kugimiya, S.; Sato, S.; Miyata, O.; Yonese, M. *Langmuir* **2000**, *16*, 4272−4278.
(79) Galeska, I.; Hickey, T.; Moussy, F.; Kreutzer, D.; Papadimitrakopoulos, F. *Biomacromolecules* **2001**, *2*, 1249−1255.
(80) Forzani, E. S.; Solis, V. M.; Ernesto, J. *Anal. Chem.* **2000**, *72*, 5300−5307.
(81) Calvo, E. J.; Battaglini, F.; Danilowicz, C.; Wolociuk, A.; Otero, M. *Faraday Discuss.* **2000**, *116*, 47−65.
(82) Calvo, E. J.; Etchenique, R.; Pietrasanta, L.; Danilowicz, C.; Wolociuk, A. *Anal. Chem*. **2001**, *73*, 1161−1168.
(83) Santos, J. P.; Welsh, E. R.; Gaber, B. P.; Singh, A. *Langmuir* **2001**, *17*, 5361−5370.
(84) Ram, M. K.; Bertoncello, P.; Ding, H.; Paddeu, S.; Nicolini, C. *Biosens. Bioelectron.* **2001**, *16*, 849−856.
(85) Wang, Y.; Wallace, E.; Walton, A.; Bathia, G.; Park, M.; Advincula, R. *Polym. Prep*. **2000**, *41*, 1026−1017.
(86) Baba, A.; Kaneko, F.; Advincula, R. *Colloids Surf.* **2000**, *173*, 39−49.
(87) Hasegawa, T.; Kazunori, M.; Katsuhiko, A.; Kazukiyo, K. *Macromolecules* **2000**, *33*, 2772−2775.
(88) Picart, C.; Lavalle, P.; Cuisinier, F. J.; Decher, G.; Schaaf, P.; Voegel, J. C. *Langmuir* **2001**, *17*, 7414−7424.
(89) Nakata, S.; Kido, N.; Hayashi, M.; Hara, M.; Sasabe, H.; Sugawara, T.; Matsuda, T. *Biophys. Chem.* **1996**, *62*, 63−72.
(90) Hook, F.; Rodahl, M.; Brzezinski, P.; Kasemo, B. *Langmuir* **1998**, *14*, 729−734.
(91) Hook, F.; Kasemo, B.; Nylander, T.; Fant, C.; Sott, K.; Elwing, H. *Anal. Chem.* **2001**, *73*, 5796−5804.
(92) Sadik, O.; Cheung, M. *Talanta* **2001**, *55*, 929−941.
(93) Briseno, A. L.; Song, F.; Baca, A. J.; Zhou, F. *J. Electroanal. Chem.* **2001**, *513*, 16−24.
(94) Kobayashi, A.; Sato, Y.; Mizutani, F. *Biosci. Biotechnol. Biochem*. **2001**, *65*, 2392−2396.
(95) Kaneda, H.; Shinotsuka, K.; Kobayakawa, T.; Saiton, S.; Okakata, Y. *J. Inst. Brew*. **2000**, *106*, 305−309.
(96) Hepel, M. *J. Electroanal. Chem*. **2001**, *509*, 90−106.
(97) Fukuoka, S.; Karube, I. *Appl. Biochem. Biotechnol.* **1994**, *49*, 1−9.
(98) Chang, H. C.; Yang, C. C.; Yeh, T. M. *Anal. Chim. Acta* **1997**, *340*, 49−54.
(99) Liebau, M.; Hildebrand, A.; Neubert, R. H. H. *Eur. Biophys. J*. **2001**, *30*, 42−52.
(100) Vikinge, T. P.; Hansson, K. M.; Sandstrom, P.; Liedberg, B.; Lindahl, T. L.; Lundstrom, I.; Tengvall, P.; Hook, F. *Biosens. Bioelectron.* **2000**, *15*, 605−613.
(101) Fawcett, N.; Evans, J. A.; Chien, L.; Flowers, N. *Anal. Lett.* **1988**, *21*, 1099−1114.
(102) Ito, K.; Hashimoto, K.; Ishimori, Y. *Anal. Chim. Acta* **1996**, *327*, 29−35.
(103) Towery, R. B.; Fawcett, N. C.; Zhang, P.; Evans, J. A. *Biosens. Bioelectron.* **2001**, *16*, 1−8.
(104) Okahata, Y.; Nikura, K.; Furusawa, H.; Matsuno, H. *Anal. Sci*. **2000**, *16*, 1113−1119.
(105) Su, H.; Yang, M.; Kallury, K. M. R.; Thompson, M. *Analyst* **1993**, *118*, 309−312.
(106) Furtado, M.; Thompson, M. *Analyst* **1998**, *123*, 1937−1945.
(107) Su, H.; Chong, S.; Thompson, M. *Langmuir* **1996**, *12*, 2247−2255.
(108) Hoeoek, F.; Ray, A.; Norden, B.; Kasemo, B. *Langmuir* **2002**, in press.
(109) Su, H.; Williams, P.; Thompson, M. *Anal. Chem*. **1995**, *67*, 1010−1013.
(110) Wang, Y.; Farrell, N.; Burgess, J. *J. Am. Chem. Soc*. **2001**, *123*, 5576−5577.
(111) Pope, L.; Allen, S.; Davies, M.; Roberts, C.; Tendler, S.; Williams, P. *Langmuir* **2002**, in press.
(112) Furtado, M.; Su, H.; Thompson, M.; Mack, D. P.; Hayward, G. L. *Anal. Chem*. **1999**, *71*, 1167−1175.
(113) Matsuno, H.; Niikura, K.; Okahata, Y. *Biochemistry* **2001**, *40*, 3615−3622.
(114) Andersson, M.; Sellborn, A.; Fant, C.; Gretzer, C.; Elwing, H. *J. Biomat. Sci., Polym. Ed.* **2002**, *13*, 907−918.
(115) Sellborn, A.; Andersson, M.; Fant, C.; Gretzer, C.; Elwing, H. *Colloids Surf. B Biointerfaces* **2002**, *27*, 295−301.
(116) Yan, F.; Sadik, O. *Anal. Chem*. **2001**, *73*, 5272−5280.
(117) Matsuno, H.; Niikura, K.; Okahata. *Eur. J. Chem*. **2001**, *75*, 3305−3312.
(118) Thompson, M.; Arthur, G. L.; Dhaliwal, G. K. *Anal. Chem*. **1986**, *58*, 1206−1209.
(119) Muratsugu, M.; Kurosawa, S.; Kamo, N. *Anal. Chem*. **1992**, *64*, 2483−2487.
(120) Ghouechian, H. O.; Kamo, N.; Hosokawa, T.; Akitaya, T. *Talanta* **1994**, *41*, 401−406.

(121) Imai, S.; Mizuno, H.; Suzuki, M.; Takeuchi, T.; Tamiya, E.; Mashige, F.; Ohkubo, A.; Karube, I. *Anal. Chim. Acta* **1994**, *292*, 65−70.
(122) Vaughan, R. D.; O'Sullivan, C. K.; Guilbault, G. G. *Enzyme Microbial Technol.* **2001**, *29*, 636−638.
(123) Sakti; Hauptmann, P.; Zimmerman, B.; Buhling, F.; Ansorge, S. *Sens. Actuators, B* **2001**, *78*, 257−262.
(124) Fung, Y. S.; Wong, Y. Y. *Anal. Chem.* **2001**, *73*, 5302−5309.
(125) Eun, A. J.; Huang, L.; Chew, F. T.; Li, S. F.; Wong, S. M. *J. Virol. Methods* **2002**, *99*, 71−79.
(126) Zhou, X.; Liu, L.; Hu, M.; Wang. L.; Hu, J. *J. Pharm. Biomed. Anal*. **2002**, *27*, 341−345.
(127) Aizawa, H.; Kurosawa, S.; Tanaka, M.; Wakeda, S.; Talib, Z.; Park, J. W.; Yoshimoto, M.; Muratsugu, M.; Hilborn, J.; Miyake, J.; Tanaka, H. *Mater. Sci. Eng. C* **2001**, *17*, 127−132.
(128) Ebara, Y.; Okahata, Y. *J. Am. Chem. Soc*. **1994**, *116*, 11209−11212.
(129) Chang, H. C.; Yang, C. C.; Yeh, T. M. *Anal. Chim. Acta* **1997**, *340*, 49−54.
(130) Uzawa, H.; Kamiya, S.; Minoura, N.; Dohi, H.; Nishida, Y.; Taguchi, K.; Yokoyama, S.; Mori, H.; Shimizu, T.; Kobayashi, K. *Biomacromolecules* **2002**, *3*, 411−414.
(131) Sato, T.; Serizawa, T.; Okahata, Y. *Biochim. Biophys. Acta* **1996**, *1285*, 14−20.
(132) Uttenthaler, E.; Schraml, M.; Mandel, J.; Drost, S. *Biosens. Bioelectron.* **2001**, *16*, 735−743.
(133) Dultsev, F. N.; Speight, R. E.; Fiorini, M. T.; Blackburn, J. M.; Abell, C.; Ostanin, V. P.; Klenerman, D. *Anal. Chem.* **2001**, *73*, 3935−3939.
(134) Cooper, M. A.; Duitsev, F. N.; Minson, T.; Ostanin, V. P.; Abell, C.; Klenerman, D. *Nature Biotechnol.* **2001**, *19*, 833−837.
(135) Eun, A. J. C.; Huang, L.; Chew, F. T.; Sam, F. Y.; Wong, S. K. *J. Virol. Methods* **2002**, *99*, 71−79.
(136) Otto, K.; Elwing, H.; Hermansson, M. *J. Bacteriol.* **1999**, *181*, 5210−5218.
(137) Matsuda, T.; Kishida, A.; Ebato, H.; Okahata, Y. *ASAIO J.* **1992**, *38*, 171−173.
(138) Redepenning, J.; Schlesinger, T. K.; Mechalke, E. J.; Puleo, D. A.; Bizios, R. *Anal. Chem*. **1993**, *65*, 3378−3381.
(139) Gryte, D. M.; Ward, M. D.; Hu, W. S. *Biotechnol. Prog.* **1993**, *9*, 105−108.
(140) Nivens, D. E.; Chambers, J. Q.; Anderson, T. R.; White, D. C. *Anal. Chem*. **1993**, *65*, 65−69.
(141) Muratsugu, M.; Romanschin, A. D.; Thompson, M. *Anal. Chim. Acta* **1997**, *342*, 23−29.
(142) Wegener, J.; Janshoff, A.; Galla, H. J. *Eur. Biophys. J.* **1998**, *28*, 26−37.
(143) Fredriksson, C.; Kihlman, S.; Rodahl, M.; Kasemo, B. *J. Mater. Sci. Mater. Med.* **1998**, *9*, 785−788.
(144) Cans. A. S.; Hook, F.; Shupliakov, O.; Ewing, A. G.; Eriksson, P. S.; Brodin, L.; Orwar, O. *Anal. Chem*. **2002**, *73*, 5805−5811.
(145) Wegener, J.; Seebach, J.; Janshoff, A.; Galla, H. J. *Biophys. J.* **2000**, *78*, 2821−2833.
(146) Zhou, T.; Braunhut, S. J.; Medeiros, D.; Marx, K. A. *Tissue Eng. Symp.: Mater. Res. Soc.* **1999**, *550*, 177−182.
(147) Marx, K. A.; Zhou, T.; Schulze, H.; Montrone, A.; Braunhut, S. J. *Biosens. Bioelectron.* **2001**, *16*, 773−782.
(148) Marx, K. A.; Zhou, T.; Montrone, A.; Braunhut, S. J. In Materials Research Society Symposium: Advanced Biomaterials-Characterization, Tissue Engineering and Complexity; Materials Research Society, Pittsburgh, PA, 2002; Vol. 711, pp 125−132.
(149) Samoylov, A.; Samoylov, T. I.; Pithirana, S. T.; Glota, L. P.; Vodyanoy, V. J. *J. Mol. Recognit.* **2002**, *15*, 197−203.
(150) Patolsky, F.; Zayats, M.; Katz, E.; Willner, I. *Anal. Chem*. **1999**, *71*, 3171−3180.
(151) Lasalles, N.; Mailley, P.; Vieel, E.; Livache, T.; Roget, A.; Corriea, J. P.; Abrantes, L. M. *J. Electroanal. Chem*. **2001**, *509*, 48−57.
(152) Patolsky, F.; Lichtenstein, A.; Willner, I. *J. Am. Chem. Soc*. **2000**, *122*, 418−419.
(153) Schakenraad, J. M.; Arends, J.; Busscher, H. J.; Dijk, F.; van Wachem, P. B.; Wildevuur, C. R. H. *Biomaterials* **1989**, *10*, 43−50.
(154) van Kooten, T. G.; Schakenraad, J. M.; van der Mei, H. C.; Busscher, H. J. *Biomaterials* **1992**, *13*, 897−904.
(155) Ruardy, T. G.; Moorlag, H. E.; Schakenraad, J. M.; Van der Mei, H. C.; Busscher, H. J. *J. Colloid Interface Sci.* **1997**, *188*, 209−217.
(156) Helle, H.; Vuoriranta, P.; Valimaki, H.; Lekkala, J.; Aaltonen, V. *Sens. Actuators B* **2000**, *71*, 47−54.
(157) Ebersole, R. C.; Foss, R. P.; Ward, M. D. *Biotechnology* **1991**, *9*, 450−455.
(158) Yao, S.; Tan, H.; Zhang, H.; Su, X.; Wei, W. *Biotechnol. Prog*. **1998**, *14*, 639−644.
(159) Peng, H.; Zhang, Y.; Xie, Q.; Nie, L.; Yao, S. *Analyst* **2001**, *126*, 189−194.
(160) Marx, S.; Kaushansky, N.; Gratziany, N.; Barness, I.; Liron, Z. *Biosens. Bioelectron.* **2001**, *16*, 239−244.
(161) Long, Y.; Liu, Y.; Lei, L.; Nie, L.; Yao, S. *Analyst* **2001**, *126*, 1090−1094.
(162) Yao, S.; Peng, H.; Liang, C.; Wu, Y.; Nie, L. *Anal. Sci*. **2000**, *16*, 211−215.
(163) Tan, Y.; Peng, H.; Liang, C.; Yao, S. *Sens. Actuators B* **2001**, *73*, 179−184.
(164) Kugiyama, A.; Yoneyama, H.; Takeuchi, T. *Electroanalysis* **2000**, *2*, 1322−1326.
(165) Peng, H.; Liang, C.; Zhou, A.; Zhang, Y.; Xie, Q.; Yao, S. *Anal. Chim. Acta* **2000**, *423*, 221−228.
(166) Haupt, K.; Noworyta, K.; Kutner, W. *Anal. Commun*. **1999**, *36*, 391−193.
(167) Cao, L.; Zhou, X. C.; Li, S. F. Y. *Analyst* **2001**, *126*, 184−188.
(168) Chance, J. J.; Purdy, W. C. *Anal. Lett.* **1999**, *32*, 1751−1760.
(169) Ward, M. D.; Lin, Z.; Yip, C. M.; Scott, J. *Anal. Chem*. **1993**, *65*, 1546−1551.
(170) Zimmerman, B.; Lucklum, R.; Hauptmann, P.; Rabe, J.; Buttgenbach, S. *Sens. Actuators B* **2001**, *76*, 47−57.
(171) Van Noort, D.; Rani, R.; Mandenius, C. F. *Mikrochim. Acta* **2001**, *136*, 49−53.
(172) Zhao, H.; Lin, L.; Tang, J.; Duan, M.; Jiang, L. *Chin. Sci. Bull*. **2001**, *46*, 1074−1077.
(173) Ghafouri, S.; Thompson, M. *Analyst* **2001**, *126*, 2159−2167.
(174) Patolsky, F.; Lichtenstein, A.; Willner, I. *Nature Biotechnol.* **2001**, *19*, 353−257.
(175) White, R. M. *1998 IEEE Int. Frequency Control Symp.* **1998**, 587−594.
(176) Wang, A. W. *TRANSDUCERS '97, 9th Int. Conf. Solid State Sens. Actuators* **1997**, 191.

BM020116I